

A versatile silica nanoparticle platform for induction of T cell responses – applied for therapeutic vaccination against HPV16 E6/E7-positive tumors in MHC-humanized mice

Sebastian Kruse, Lia T. Fricke, Samantha Zotnick, Ann-Katrin Schlosser, Agnieszka K. Grabowska, Eva Feidt, Philipp Uhl, Ellen Junglas, Jonas D. Förster, Josephine Blersch, Philip Denner, Manina Günter, Stella E. Autenrieth, Eugenio Fava, Walter Mier, Armin Kübelbeck & Angelika B. Riemer

To cite this article: Sebastian Kruse, Lia T. Fricke, Samantha Zotnick, Ann-Katrin Schlosser, Agnieszka K. Grabowska, Eva Feidt, Philipp Uhl, Ellen Junglas, Jonas D. Förster, Josephine Blersch, Philip Denner, Manina Günter, Stella E. Autenrieth, Eugenio Fava, Walter Mier, Armin Kübelbeck & Angelika B. Riemer (2025) A versatile silica nanoparticle platform for induction of T cell responses – applied for therapeutic vaccination against HPV16 E6/E7-positive tumors in MHC-humanized mice, *Oncolmunology*, 14:1, 2548002, DOI: [10.1080/2162402X.2025.2548002](https://doi.org/10.1080/2162402X.2025.2548002)

To link to this article: <https://doi.org/10.1080/2162402X.2025.2548002>



© 2025 The Author(s). Published with license by Taylor & Francis Group, LLC.



[View supplementary material](#)



Published online: 25 Aug 2025.



[Submit your article to this journal](#)



Article views: 856








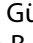







[View related articles](#)



[View Crossmark data](#)

A versatile silica nanoparticle platform for induction of T cell responses – applied for therapeutic vaccination against HPV16 E6/E7-positive tumors in MHC-humanized mice

Sebastian Kruse ^{a,b,c,*}, Lia T. Fricke ^{a,b,d,*}, Samantha Zottnick ^{a,b}, Ann-Katrin Schlosser ^{a,b,e}, Agnieszka K. Grabowska^c, Eva Feidt^c, Philipp Uhl ^{f,g}, Ellen Junglas^c, Jonas D. Förster ^{a,b,e}, Josephine Blersch ^h, Philip Denner ^h, Manina Günter ⁱ, Stella E. Autenrieth ⁱ, Eugenio Fava ^h, Walter Mier ^g, Armin Kübelbeck^c, and Angelika B. Riemer ^{a,b}

^aDivision of Immunotherapy & Immunoprevention, German Cancer Research Center (DKFZ), Heidelberg, Germany; ^bMolecular Vaccine Design, German Center for Infection Research (DZIF), Partner Site Heidelberg, Heidelberg, Germany; ^cSILVACX, Life Science Inkubator GmbH, Bonn, Germany; ^dFaculty of Medicine, Heidelberg University, Heidelberg, Germany; ^eFaculty of Biosciences, Heidelberg University, Heidelberg, Germany; ^fInstitute of Pharmacy and Molecular Biotechnology, Department of Pharmaceutical Technology and Biopharmacy, Heidelberg University, Heidelberg, Germany; ^gDepartment of Nuclear Medicine, Heidelberg University Hospital, Heidelberg, Germany; ^hLaboratory Automation Technologies (CRFS-LAT), German Center for Neurodegenerative Diseases (DZNE), Bonn, Germany; ⁱDendritic Cells in Infection and Cancer, German Cancer Research Center (DKFZ), Heidelberg, Germany

ABSTRACT

Therapeutic vaccines represent a promising treatment option for (pre)cancerous lesions, such as human papillomavirus-induced malignancies. They act via administration of tumor-specific antigens, leading to induction of antigen-specific cytotoxic T cell responses. However, vaccination efficiency is often limited when the antigen is administered alone, due to antigen instability and inefficient uptake by antigen-presenting cells (APCs). To address these limitations, nanoparticle-based vaccine delivery systems are currently under investigation. Here, we present a novel silica nanoparticle (SiNP)-based vaccine delivery platform that can be applied for the treatment of various diseases and cancer types. We show that surface-functionalized SiNPs are non-cytotoxic and quickly taken up by APCs. Incorporation of a linker/solubilizer sequence N-terminal of the epitope allows attachment of peptides regardless of their solubility as well as efficient processing and surface presentation by APCs. Whole-body distribution studies confirmed retention of the antigen at the injection site and decelerated excretion when connected to SiNPs. Furthermore, treatment with SiNPs, especially when combined with the adjuvant poly(I:C), resulted in activation of dendritic cells capable of priming CD8⁺ T cells. In C57BL/6 and MHC-humanized A2.DR1 mice, the SiNP-based vaccinations induced epitope-specific CD8⁺ T cells. Moreover, they exhibited anti-tumor activity and provided a survival benefit in a tumor model using HPV16 E6/E7-expressing PAP-A2 cells. Thus, the novel SiNP platform represents a promising new vehicle for therapeutic vaccine delivery.

ARTICLE HISTORY



Received 20 February 2025
Revised 7 August 2025
Accepted 10 August 2025

KEYWORDS


Amorphous silica nanoparticles; cervical cancer; therapeutic vaccination; MHC-humanized mouse model; A2.DR1; human papillomavirus (HPV); cancer immunotherapy

Introduction

Among various immunotherapeutic strategies, therapeutic vaccination represents a promising approach for the treatment of (pre-)cancerous lesions. It is based on the administration of tumor-specific antigens, their delivery to and surface presentation by professional antigen-presenting cells (APCs), such as dendritic cells (DCs), and subsequent induction of antigen-specific CD8⁺ cytotoxic T cell responses.^{1,2} The antigen can be administered in the form of DNA, RNA, peptides, and proteins, and can encompass a whole protein sequence, synthetic long peptides (SLPs), or only a minimal epitope.¹ Usually, the given antigen is additionally combined with adjuvants, such as mineral salts or Toll-like receptor (TLR) agonists, necessary for proper activation of APCs for

CONTACT Angelika B. Riemer  a.riemer@dkfz.de  Division of Immunotherapy & Immunoprevention, German Cancer Research Center (DKFZ), Im Neuenheimer Feld 280, 69120 Heidelberg, Germany

*Equal contribution.

 Supplemental data for this article can be accessed online at <https://doi.org/10.1080/2162402X.2025.2548002>

© 2025 The Author(s). Published with license by Taylor & Francis Group, LLC.

This is an Open Access article distributed under the terms of the Creative Commons Attribution-NonCommercial License (<http://creativecommons.org/licenses/by-nc/4.0/>), which permits unrestricted non-commercial use, distribution, and reproduction in any medium, provided the original work is properly cited. The terms on which this article has been published allow the posting of the Accepted Manuscript in a repository by the author(s) or with their consent.

efficient triggering of adaptive immune responses.³ Nevertheless, administration of free antigen often results in only limited effectivity due to various obstacles, such as antigen instability and inefficient uptake by APCs.^{1,4,5}

In recent years, the focus has therefore shifted toward the development of nanoparticle (NP)-based vaccine delivery systems. NPs display a common characteristic of ranging between 1 and 100 nm in size⁶ and can be categorized into subclasses according to the material they are made of, such as lipid-based, polymeric, and inorganic NPs.⁷ Recently published therapeutic NP vaccination approaches mostly focused on lipid-based vaccines, including lipid nanoparticles,^{8,9} lipoplex mRNA constructs,^{10,11} and various amphiphilic liposomes,^{12–14} some of which have already been tested in clinical studies.^{15,16} Nevertheless, also polymeric and inorganic NPs have various useful characteristics, which is why they have received increasing attention in recent years.¹⁷ Especially, silica nanoparticles (SiNPs) are well-suited for biomedical applications, due to the ease of controlling and achieving uniformity of their size and shape, their large surface area, high loading capacity, and good biocompatibility.^{18,19} Due to their easily modifiable surfaces and their stability at various conditions, such as different temperatures and pH values, they are one of the most widely used nanomaterials for numerous applications including drug delivery as well as biomedical imaging.^{18–20} Also as therapeutic cancer vaccine platform, SiNPs have been explored and shown promising results in preclinical proof-of-concept studies.²¹ However, most platforms have not yet been further developed regarding the applicability to a clinically relevant disease or cancer type.

A clinically relevant setting in which the development of a therapeutic vaccine is urgently needed are human papillomavirus (HPV)-induced malignancies. There are at least 12 known oncogenic (so-called high-risk) types of HPV,²² all of which are transmitted through sexual activity. They drive oncogenesis through the expression of the two viral oncoproteins E6 and E7. E6 causes degradation of p53, while E7 acts by inhibiting pRb, together leading to uncontrolled cell proliferation and resistance to cell death.²³ Accordingly, these oncoproteins are indispensable for establishing and maintaining the malignant phenotype and therefore need to be expressed at all stages of cancer development.²³ Peptides derived from E6 and E7 are consequently also HLA-presented on the cell surface, making them ideal targets for therapeutic vaccination.^{23,24} HPV causes cancers in the anogenital and head and neck region, overall accounting for approximately 5% of cancer cases worldwide.^{25,26} Of all known high-risk HPV types, HPV16 is the most prevalent, being responsible for more than 60% of all cervical and more than 85% of HPV-induced head and neck cancer cases.^{27,28} To reduce the HPV-related cancer burden, several intervention strategies are available: Prophylactic vaccinations aim at preventing an infection with high-risk HPV types in the first place, and regular screenings are performed to identify precancerous lesions. However, in 2023, only 27% of girls worldwide were estimated to have received at least a first vaccine dose, and vaccination rates in boys are even lower.²⁹ Regular screenings are only available for cervical cancer, leaving other HPV-related cancer types often undetected until they reach advanced stages.³⁰ The current standard of care, which typically includes surgery, chemotherapy, and radiation, is often associated with significant side effects and a diminished quality of life.³⁰ In recent years, immune checkpoint blockade has been approved as another treatment option for HPV-associated malignancies, however showing only limited response rates.³¹ Thus, a new, efficacious treatment option targeting HPV-associated lesions and cancers is urgently needed. For this reason, numerous groups have been working on the development of a therapeutic HPV-targeting vaccine over the past decades. However, none of the approaches have shown sufficient success to be approved for clinical use.

Here, we present a safe and biodegradable SiNP-based vaccine delivery platform. Our SiNPs were efficiently taken up and processed by APCs, resulting in MHC-mediated presentation of the loaded epitope on the APC surface. In addition, treatment of APCs with SiNPs, especially when combined with the adjuvant poly(I:C), resulted in activation of DC subsets capable of CD8⁺ T cell priming. *In vivo* studies proved that vaccination with SiNPs successfully induced epitope-specific CD8⁺ T cell responses, which we demonstrated in two different model systems, using the ovalbumin (OVA)-derived epitope SIINFEKL as well as the HPV16 E7-derived epitope YMLDLQPET. Furthermore, the SiNP-induced YMLDLQPET-specific immune response elicited anti-tumor effects, proving the suitability of our SiNP platform for therapeutic vaccination against HPV16-mediated malignancies.

Material and methods

SiNP synthesis, surface modification, and addition of peptides and poly(I:C)

All SiNP constructs were produced by SILVACX at Life Science Inkubator GmbH (Bonn, Germany). Amorphous, spherical SiNPs were synthesized via the Stöber process³² at 26°C through mixing of tetraethyl orthosilicate (TEOS) with ethanol and 0.325–0.35% ammonia water, depending on the desired SiNP diameter. Higher ammonia concentrations generate larger particles. After 1 h, ethanol and ammonia were removed via distillation and subsequent membrane dialysis.

For SiNP surface arginylation, 10 equivalents of arginine and one equivalent of (3-triethoxysilyl) propylsuccinic anhydride (CAS No. 93642-68-3) were added under stirring at room temperature (RT). The excess equivalents of arginine ensured a buffered alkaline pH value between 10.5 and 11. Subsequently, membrane dialysis was performed to remove excess arginine and formed ethanol.

For SiNP surface phosphorylation, diethylphosphatoethyltriethoxysilane (CAS No. 757-44-8) was added at RT to the SiNP suspension and incubated for 24 h. Afterward, additional concentrated ammonia water was added. The reaction mixture was transferred into a pressure-resistant closed bottle and heated up to 80°C. Subsequently, ethanol and ammonia were removed via distillation and subsequent membrane dialysis.

For SiNP surface thiolation, (3-mercaptopropyl)triethoxysilane (CAS No. 14814-09-6) was added at RT to the SiNP suspension and incubated for 24 h. Afterward, ethanol and ammonia were removed by distillation and subsequent membrane dialysis.

Peptides and poly(I:C) were bound to the surface modified SiNPs by mixing all components in water. All nanosuspensions were subsequently sterile filtered with a 0.2 µm filter.

Dynamic light scattering

Particle diameters and polydispersity index (PDI) were assessed by dynamic light scattering (DLS) by diluting 20 µl of the SiNP formulation with 1 ml PBS and measuring it using a ZetaSizer Nano (Malvern Corp.).

Transmission electron microscopy

Carbon-coated 200 mesh copper grids were pre-treated with argon plasma for 45 sec using a BALTEC MED-020 coating system. 6 µl of a SiNP solution with a concentration of 20 mg/ml was added onto the grid and incubated for 5 min at RT. The grid was afterward treated with one drop of 2% uranyl acetate for 2–3 sec, another drop of 2% uranyl acetate for 25 sec, and was then washed three times with a drop of water for 15 sec. The excess liquid was removed, and the grid was allowed to dry. Pictures were taken using a JEOL-2200FS transmission electron microscope.

Toxicity of SiNPs in human PBMCs

Ex vivo toxicity of SiNPs was assessed as described by Bliersch et al.³³ Briefly, PBMCs were isolated by density gradient centrifugation. Subsequently 60,000 PBMCs/well were incubated with different SiNPs in different concentrations for 4 h. For the last 30 min, propidium iodide (PI) in a concentration of 5 µg/ml was added. Afterward, cells were washed with PBS containing 1% FBS, fixed with 4% paraformaldehyde (PFA) for 15 min, and analyzed by high-content imaging. For data presentation, the mean of 16 image fields for each condition and a four-parametric logistic regression was calculated.

Cell lines

The DC2.4 cell line³⁴ was supplied by K. Rock (Dana-Farber Cancer Institute) and was maintained in RPMI-1640 medium (Gibco) supplemented with 10% FCS (Gibco), 1% penicillin/streptomycin (Sigma-Aldrich), 1% non-essential amino acid solution (Gibco), 2 mM L-glutamine (Thermo Scientific), 10 mM HEPES buffer (Gibco), and 54 µM β-mercaptoethanol (Gibco). THP1 cells were purchased from ATCC

(ATCC no. TIB-202) and were maintained in RPMI-1640 medium supplemented with 10% FCS, 1% penicillin/streptomycin, 2 mM L-glutamine, 10 mM HEPES buffer, 1 mM sodium pyruvate (Corning), and 50 μ M β -mercaptoethanol. C33A and CaSki cells were purchased from ATCC (ATCC no. HTB-31 and CRL-1550) and were maintained in DMEM (Sigma) supplemented with 10% FCS, 1% penicillin/streptomycin, and 2 mM L-glutamine. PAP-A2 cells were generated in the Riemer lab.³⁵ They express tagged versions of the HPV16 proteins E6 and E7 and are syngeneic to A2.DR1 mice. PAP-A2 cells were cultured in DMEM supplemented with 10% FCS, 10 mM HEPES buffer, 50 μ M β -mercaptoethanol, 2 mM L-glutamine, 1 mM sodium pyruvate, and 2 μ g/ml puromycin (Sigma).

SIINFEKL presentation assay

DC2.4 was incubated in flat-bottom 96-well plates with indicated SiNP constructs containing 100 μ g/ml SiNPs and 1.25 μ M SIINFEKL for 6–48 h. After incubation, medium was taken off, wells were washed once with PBS, and cells were harvested using Trypsin/EDTA (Sigma-Aldrich). Subsequently, Fc receptors were blocked with anti-CD16/CD32 blocking antibody (BD Biosciences) at a concentration of 10 μ g/ml for 10 min at 4°C. Fc-blocking solution was discarded after centrifugation, and ZombieAqua (Biolegend, 1:200) for dead cell exclusion and anti-SIINFEKL/H-2Kb AB conjugated to PE-Cy7 (clone 25-D1.16, Invitrogen, 1:100) was added in PBS with 0.1% BSA, and cells were incubated for 30 min at 4°C. Samples were washed three times with PBS with 0.1% BSA. Stained samples were analyzed on a BD FACSCanto II flow cytometer.

THP-1 presentation assay

2×10^7 THP-1 cells were treated with SiNP solution containing 100 μ g/ml SiNPs and 1.25 μ M YMLDLQPET (HPV16 E7/11–19) for 2 h. Afterward, cells were washed twice with PBS and incubated for another 4 h until they were harvested and frozen for subsequent immunopeptidomics analysis.

Immunoprecipitation of HLA-displayed peptides and LC-MS

Immunoprecipitation of HLA-displayed peptides and mass spectrometric analysis was performed as described previously.^{36,37} Cell pellets were lysed, and HLA:peptide complexes were immunoprecipitated using a pan-HLA class I monoclonal antibody (clone W6/32) crosslinked to Protein A Sepharose 4B beads (Invitrogen) in 96-well format. Peptides were desalted using SepPak tC18 plates (Waters) with an additional forced oxidation step. Peptide elution was performed with 28% ACN, and samples were dried by vacuum centrifugation. For MS analysis, samples were dissolved in 10.5 μ L 5% ACN, 0.1% TFA spiked with 50 fmol Pierce Peptide Retention Time Calibration Mixture (Thermo Fisher Scientific). Samples were analyzed using an UltiMate 3000 RSLCnano system coupled to an Orbitrap Exploris 480 (Thermo Fisher Scientific). For chromatographic separation, peptides were first loaded onto a trapping cartridge (Acclaim PepMap 100 C18 μ -Precolumn, 5 μ m, 300 μ m i.d. \times 5 mm, 100 Å; Thermo Fisher Scientific) and then eluted and separated using a nanoEase M/Z Peptide BEH C18 130A 1.7 μ m, 75 μ m \times 200 mm (Waters). MS raw data were analyzed with the Skyline software. Data visualization was performed using in-house developed R scripts.

MS1 data were recorded with a resolution of 120,000 at 200 m/z with 3×10^6 AGC target and 25 ms maximum IT. MS2 data were acquired with PRM scans using a resolution of at least 120,000 at 200 m/z. The normalized AGC target was set to 1000% (or 1×10^6) and 25 ms maximum IT. The dynamic RT feature using the PRTC mixture was active.

LC-MS data were analyzed using Skyline software.³⁸ Transitions were extracted in centroided mode with 6 ppm mass tolerance. Detected peaks were manually curated to exclude transitions not adhering to the peak indicated by dominant transitions and to adjust integration boundaries accordingly. The normalized spectral contrast angle (NSA)³⁹ was used to determine the similarity of the acquired signal to the synthetic reference and a threshold of 0.85 was required to confirm detection. Data visualization was performed using in-house developed R scripts.⁴⁰

Immunofluorescence

DC2.4 cells were incubated on coverslips in 24-well plates with indicated SiNP constructs in a concentration of 50 µg/ml SiNP and 1 µg/ml epitope in 300 µl medium/well for 1–8 h. 1 h before the end of incubation, 10 µl lysotracker red (Invitrogen) was added to a final concentration of 0.1 µM/well. At the end of incubation, cells were washed three times with PBS and fixed with 300 µl of 4% PFA in PBS by incubation for 10 min at RT in the dark. Afterward, cells were washed thrice with PBS, stained for DAPI with 10 µl antifade reagent (Invitrogen) and sealed after 24 h with clear nail varnish. Confocal microscopy was performed with a Zeiss LSM 710 ConfoCor 3 and pictures taken with the 63x objective.

Animals

Adult female Wistar rats (200–250 g) were purchased from Janvier Labs (Le Genest-Saint-Isle, France). Vaccination experiments using 6–8 week old female C57BL/6 mice were performed at Charles River Laboratories (Freiburg, Germany), where they were kept under specific pathogen-free conditions. A2.DR1 mice were provided by the Institut Pasteur^{41–44} and bred in-house under specific pathogen-free conditions. For experiments, age-matched groups of 6–20 week-old female mice were used. All national and institutional guidelines were followed and experiments were approved by Regierungspräsidium Karlsruhe (approval numbers G143/18, G189/18, and G199/21). We have adhered to ARRIVE guidelines on reporting of animal *in vivo* experiments.

DC activation assay

Single-cell suspensions from spleens of C57BL/6 and A2.DR1 mice were prepared as previously described by Autenrieth et al.⁴⁵ 3×10^6 splenocytes were seeded in 12-well plates in RPMI-1640 medium supplemented with 10% FBS, 2 mM L-glutamine, 100 U/ml penicillin/streptomycin, 50 µM 2-mercaptoethanol, 1 mM sodium pyruvate, 10 mM HEPES buffer, and $1 \times$ non-essential amino acids and incubated for 6 h with indicated constructs in a concentration of 100 µg/ml SiNP, 2.5 µg/ml poly(I:C) (VacciGrade™, Invivogen) and/or 1.25 µM epitope. Afterward, cells were harvested using Accutase (Merck). Cells were washed once with PBS and stained with Zombie NIR (BioLegend, 1:2000) for 1 h at 4°C. Cells were washed once with Cell Staining Buffer (Biolegend) and then incubated with hybridoma supernatant from 2.4G2 cell line producing anti-FcγRII/III mAb at 4°C for 10 min to avoid unspecific antibody binding. This was followed by extracellular staining for 1 h at 4°C using antibodies listed in Table 1 in a final volume of 100 µl. Cells were washed once with Cell Staining Buffer containing tandem stabilizer (BioLegend), and at least 1.5×10^6 cells were acquired using an Aurora flow cytometer (Cytek Bioscience) with the SpectroFlow software. Unmixing was performed in SpectroFlow using cell- or bead-based single-stain controls and unstained cells for autofluorescence subtraction. Data analysis was performed in OMIQ software (Dotmatics). Splenocytes were gated for single, live CD45⁺ leukocytes. Afterward, B cells, T cells, NK cells, and granulocytes were excluded using the markers CD19, CD3, NK1.1, and Ly6G, respectively. Next, plasmacytoid dendritic cells (pDCs), conventional dendritic cells (cDCs), and monocytes were discriminated using PDCA-1, CD11c, and Ly6C (pDCs: PDCA-1⁺; cDCs: CD11c⁺, Ly6C[−]; monocytes: CD11c[−], Ly6C⁺). cDCs were further divided into pre-cDCs (MHC II^{low}) and mature cDCs (MHC II^{high}). Mature cDCs were then split into cDC1s (XCR1⁺, CD172a[−]) and cDC2s (XCR1[−], CD172a⁺). Finally, inflammatory cDC2s (inf-cDC2) were discriminated from other cDC2 by the expression of FcεR1α. Activation was assessed by staining for CD40 and CD86.

Radiolabeling and whole-body distribution of SiNP

Radiolabeling was performed using D-tyrosine-modified peptide KKK-W-Cit-yE7/11–19 as described previously for other peptide therapeutics by Uhl et al.⁴⁶ For loading of SiNPs with radiolabeled peptide, the peptide was incubated with 25 µl of a SiNP stock solution with a concentration of 50 mg/ml and vortexed for 60 sec. To determine the whole-body distribution, Wistar rats were anaesthetized by isoflurane

Table 1. Antibodies used for DC activation assay.

Marker	Fluorochrome	Company	Clone	Final conc.
CD40	BUV737	BD Bioscience	3/23	5 µg/ml
Ly6G	Pacific Blue	BioLegend	1A8	0.625 µg/ml
CD86	BV480	BD Bioscience	PO3	5 µg/ml
CD19	BV510	BioLegend	6D5	0.625 µg/ml
NK1.1	BV510	BioLegend	PK136	2.5 µg/ml
CD317 (PDCA-1)	BV650	BioLegend	927	0.42 µg/ml
CD64	BV711	BioLegend	X54–5/7.1	2.5 µg/ml
FcεR1α	BV750	BD Bioscience	MAR-1	1.25 µg/ml
CD11c	PE/Fire640	BioLegend	QA18A72	0.17 µg/ml
CD3	PE/Fire700	BioLegend	17A2	0.625 µg/ml
MHCII	PE/Fire810	BioLegend	M5/114.15.2	0.2 µg/ml
HLA-DR	PE/Fire810	BioLegend	L243	0.08 µg/ml
CD172a	APC	BioLegend	P84	1 µg/ml
XCR1	AF647	BioLegend	ZET	2.1 µg/ml
Ly6C	APC/Cy7	BioLegend	HK1.4	0.17 µg/ml
CD45	APC/Fire810	BioLegend	30-F11	0.42 µg/ml

inhalation, and 100 µl of the free radiolabeled peptide or the SiNP-loaded radiolabeled peptide was administered by s.c. injection into the neck fold of one animal each. Scintigraphic images were recorded at different time points by a γ-camera.

Vaccination

C57BL/6 mice and A2.DR1 mice were injected s.c. with 100 µl of the indicated SiNPs or control solutions in combination with 50 µg of poly(I:C). All solutions were injected s.c. into the flank of the mice (contralateral flank in tumor-bearing mice). The specific vaccination schedules as well as the number of mice used per group are indicated in the respective figures. Group sizes were determined a priori together with the DKFZ biostatistics department.

Splenocyte isolation and intracellular cytokine staining

Vaccinated mice were sacrificed 7 days after the last injection by CO₂ inhalation and subsequent cervical dislocation and their spleens were aseptically removed. Spleens were minced with a scalpel, and splenocytes were separated through a 70 µm cell strainer. Red blood cells were lysed with ACK buffer (ammonium-chloride-potassium). 2×10^6 splenocytes were stimulated with PMA/Ionomycin (pos. ctrl.), irrelevant peptide (neg. ctrl./background), and cognate peptide, respectively, in the presence of GolgiStop (BD Biosciences) and GolgiPlug (BD Biosciences) in U-bottom 96-well plates for 5 h at 37°C and 5% CO₂. After incubation, extracellular staining was performed against CD3 (clone 145-2C11, BD Biosciences, 1:100), CD19 (clone 6D5, Thermo Fisher Scientific, 1:100), CD4 (clone RM4–5, BD Biosciences, 1:200), CD8 (clone KT15, Santa Cruz Biotechnology, 1:100) combined with ZombieAqua live/dead stain (Biolegend, 1:200). Cells were permeabilized using the BD Cytofix/Cytoperm kit (BD Biosciences) according to the manufacturer's instructions and afterward stained against IFNγ (XMG1.2, BD Biosciences, 1:200). Cells were analyzed on a BD FACSCanto II flow cytometer. Data were analyzed with FlowJo. Splenocytes were gated for single, live cells. Afterward, CD3⁺ CD8⁺ T cells were analyzed regarding IFNγ production.

Tumor inoculation

PAP-A2 cells were harvested and washed thrice with PBS. 1.5×10^6 cells per mouse were taken up in 50 µl of PBS, and 50 µl of matrigel matrix was added. The resulting solution was injected s.c. into the flank of the mouse on day 0. Tumor growth was measured, with the experimenter being blinded to group allocation, with digital calipers at least twice a week, and tumor volume was calculated according to the formula $v = 4/3\pi(0.5 \times \text{length}) \times (0.5 \times \text{width})^2$. Due to the vaccination starting early after tumor implantation, measurement of tumor size before the first vaccination was not possible. For this reason, mice were distributed into groups based only on their age and familial relationships, and not on the tumor size. Mice not forming a tumor or

sacrificed due to vaccination complications were censored in the analysis. Mice were sacrificed by CO₂ inhalation and subsequent cervical dislocation once a tumor volume of 1000 mm³ was exceeded or at signs of distress.

Statistics

GraphPad Prism 8 was used for statistical analyses. The specific statistical parameters and the statistical tests used are indicated in the figure legends.

Results

Silica nanoparticles need surface functionalization for tolerability

Amorphous, spherical SiNPs were synthesized via the conventional Stöber process through ammonia-catalyzed hydrolysis of tetraethyl orthosilicate (TEOS) in water.³² We compared uncoated SiNPs displaying hydroxyl groups (–OH) on their surface with surface-functionalized SiNPs using thiolation (–SH), arginylation (–Arg), or phosphorylation (–PO₃H₂) (Figure 1A). Synthesis via the Stöber process ensured the generation of monodisperse particles (Figure 1B) with polydispersity indices (PDI) of around 0.1, as determined via dynamic light scattering (Figure 1C and Supplementary Figure S1). This was independent of the particle size, which we chose to range between 20 nm and 40 nm in diameter (Figure 1B,C). Although silica particles can be produced in various sizes up to the μm range, we focused on a size that is ideal for transport through lymphatics and uptake by APCs.^{47,48} Potential toxicity of SiNPs was assessed *ex vivo* by determining the fraction of dead cells upon treatment of human peripheral blood mononuclear cells (PBMCs) with increasing concentrations of uncoated vs. surface-functionalized (in this case arginylated) SiNPs. Arginylated SiNPs were well tolerated at all concentrations tested (0–1,000 μg/ml), while treatment with uncoated SiNPs at a concentration of 125 μg/ml or higher resulted in severe toxicity with up to 100% cell death (Figure 1D). These results indicate that surface functionalization can abolish the toxic effects of uncoated SiNPs – an aspect that has important implications for de-risking of SiNP applications and needs to be considered in the context of safe-by-design criteria.⁴⁹ For this reason, uncoated SiNPs were excluded from further analyses.

Choice of surface functionalization, solubilizer, and linker affect epitope presentation

We next studied the SiNP epitope-loading capacity as well as uptake, processing, and surface presentation of loaded epitopes *in vitro*. We synthesized SiNPs with various surface functionalizations, solubilizers, and linkers, through which the epitope of interest was loaded onto the SiNP (Figure 2A). Dynamic light scattering revealed that SiNP-epitope solutions were stable in regard to particle size and PDI as long as the peptide load accounted for less than 7%w/w (Figure 2B,C).

To assess the effects of SiNP surface functionalization on epitope release from the particle and APC surface presentation on MHC molecules, the murine dendritic cell line DC2.4 was incubated with SiNPs, to which the H-2K^b-restricted Ovalbumin (OVA) epitope SIINFEKL was either adsorptively (SiNP-PO₃H₂~) or covalently (SiNP-SH=) bound. While it was possible to attach the epitope directly to the SiNP via adsorption, covalent attachment of SiNP and epitope necessitated a chemical compound on the epitope (methiopropamine, MPA) capable of covalently binding to the thiol groups on the SiNPs. In addition, a spacer sequence ((EGG)3-EW-Cit) was integrated to facilitate accessibility of the cleavage site. Flow cytometric analysis of H-2K^b surface-presented SIINFEKL showed that adsorptively bound epitope was released from the SiNP efficiently in DC2.4 cells, leading to significant MHC presentation. In fact, it was found to be presented on the cell surface in an almost equal measure compared to cells pulsed with free SIINFEKL (Figure 2D,E and Supplementary Figure S2). In contrast, no H-2K^b-presented SIINFEKL was detected on cells incubated with the epitope covalently linked to SiNPs, indicating no or very inefficient release from the particle. Interestingly, also cells incubated with the free epitope bound to MPA and the spacer were found to present SIINFEKL to a lesser extent compared to cells incubated with free unmodified epitope, suggesting improper cleavage of the epitope from its spacer. The difference in epitope presentation

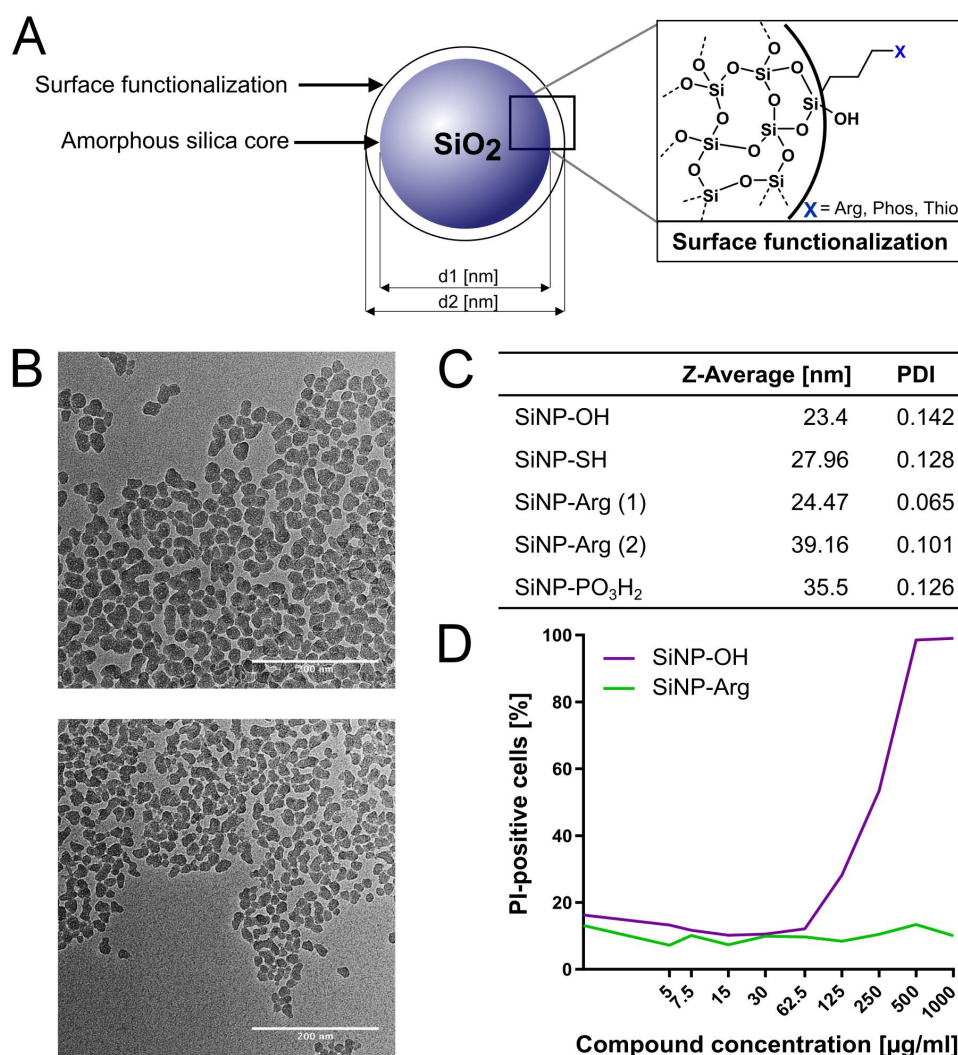


Figure 1. Physicochemical characterization and cytotoxicity assessment of SiNPs. (A) Schematic representation of the chemical structure of the amorphous SiNP core and its optional surface functionalizations. (B) Representative transmission electron microscopy (TME) images of SiNPs with diameters of 40 nm (top) and 25 nm (bottom). (C) Summary of physicochemical characteristics of SiNPs with different surface functionalizations, including size and polydispersity index (PDI). (D) Toxicity analysis of uncoated (–OH) and arginylated (–Arg) SiNPs on PBMCs as assessed by propidium iodide (PI) staining.

between adsorptive attachment and covalent conjugation to the SiNP was found to be highly statistically significant. Subsequent analyses therefore focused on phosphorylated and arginylated SiNPs, which allow loading of epitopes through adsorptive bonds.

To further optimize epitope processing and presentation, the cleavable linker tryptophan-citrullin (W-Cit) as well as two different solubilizers, consisting of either three consecutive lysines (KKK) or one arginine (R), were introduced, either N- or C-terminally of the epitope. In addition, we tested N- and C-terminal elongations of the SIINFEKL minimal epitope using the amino acids TE representing the natural sequence of the OVA protein C-terminally of SIINFEKL. Incubation of DC2.4 cells with the different constructs and subsequent flow cytometric analysis showed that incubation with the SIINFEKL minimal epitope N-terminally linked either directly to phosphorylated or arginylated SiNPs or through the KKK-W-Cit or R-W-Cit solubilizer/linker combination resulted in similar fluorescence intensities as compared to pulsing of cells with free SIINFEKL (Figure 2F), indicating proper release, processing, and surface presentation.

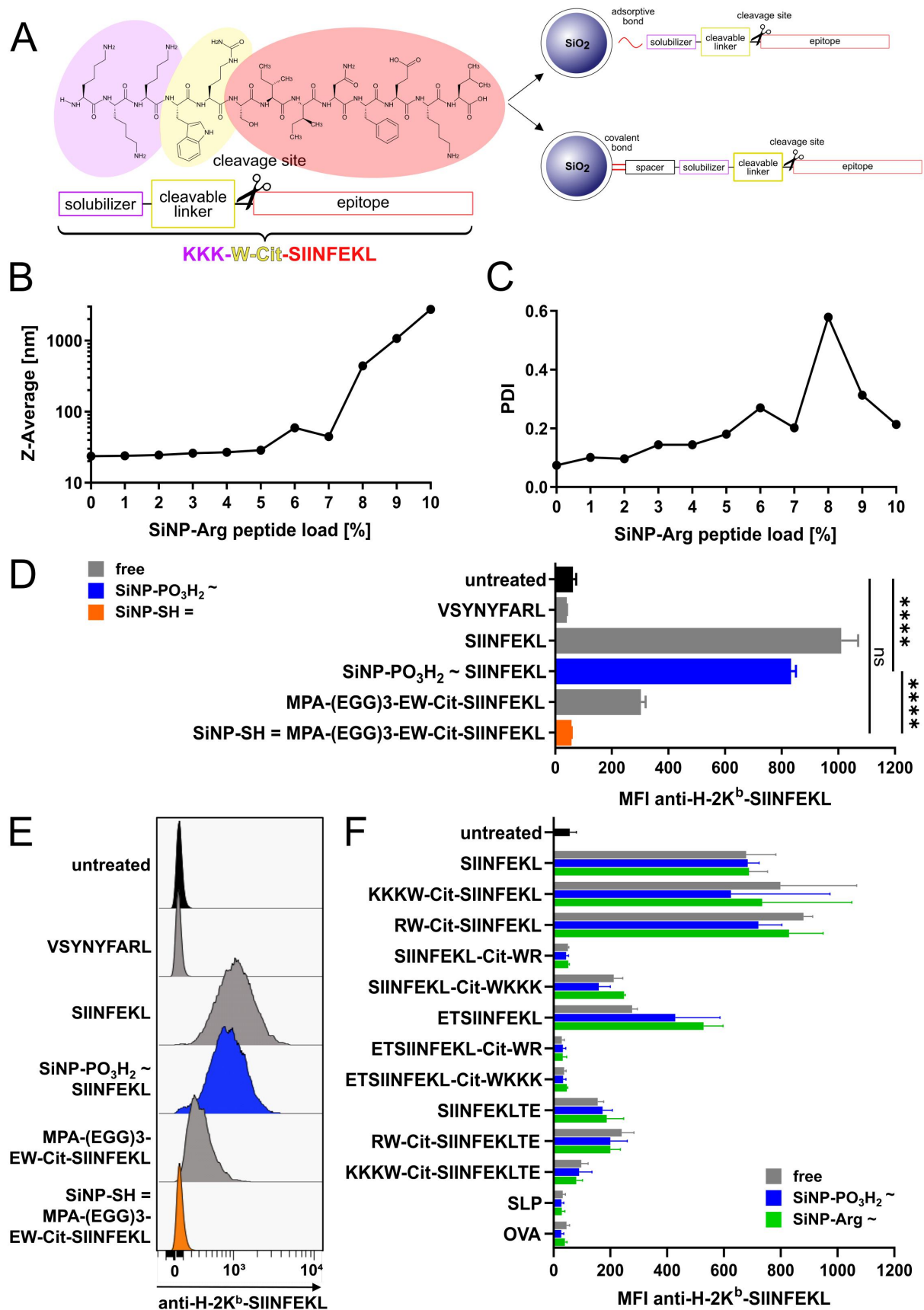


Figure 2. Optimization of SiNP-epitope constructs using different surface functionalizations and solubilizers. (A) Schematic representation of entire SiNP constructs, either using adsorptive (top) or covalent bonds (bottom). (B) SiNP size (Z-average; nm) with increasing peptide load, determined by dynamic light scattering (DLS). (C) Polydispersity index (PDI) of the SiNP

In contrast, incubation with the minimal epitope SIINFEKL, C-terminally connected to the linker or with C-terminally elongated epitopes (irrespective of the linker being N- or C-terminally placed), resulted in strongly reduced surface presentation compared to pulsing of cells with free SIINFEKL, while N-terminal elongation alone did not affect surface presentation as much. In addition, usage of the minimal epitope was clearly superior to the application of a synthetic long peptide (SLP) or the whole protein sequence (OVA), which both did not lead to SIINFEKL surface presentation. No difference was observed between treatment with free or SiNP-bound epitope, emphasizing that the SiNP itself does not negatively affect epitope processing and surface presentation, as long as the epitope is adsorptively attached to the particle and a proper cleavage site for release of the epitope is present.

Binding of epitope to SiNPs via the KKK-W-Cit solubilizer/linker combination decelerates excretion and promotes uptake by APCs

After confirming the ability of SiNP constructs to lead to surface MHC presentation of epitopes on antigen-presenting cells (APCs) *in vitro*, the *in vivo* whole-body distribution was examined in Wistar rats. After subcutaneous (s.c.) injection, isotope-labeled free epitope was cleared from the injection site within less than 4 h (Figure 3A, left). In contrast, epitope bound to arginylated SiNPs via the KKK-W-Cit solubilizer/linker combination was still detectable at the injection site even 4 h after injection (Figure 3A, right), suggesting that the attachment to SiNPs slowed down local clearance and thus may increase the chance of uptake by APCs. Eventually, the epitope was detected in the kidneys, suggesting renal excretion (Figure 3A).

For a more detailed assessment of the dynamics of SiNP uptake by APCs, DC2.4 cells treated with different fluorescently labeled SiNP-epitope constructs were monitored over time by confocal microscopy. While cells treated with SIINFEKL attached directly or via the R solubilizer to arginylated SiNPs showed only moderate presence of the epitope inside the cells, stronger signals were detected upon treatment with SIINFEKL attached via the KKK solubilizer (Figure 3B). While SiNPs were almost exclusively co-localized with lysosomes, the epitope was also detected outside of those compartments (Figure 3B), supporting the previous observations that the epitope was cleaved off efficiently, and was successfully released into the cytosol. Monitoring of SiNP-Arg~KKK-W-Cit-SIINFEKL-treated cells over time showed continuous uptake of SiNP and epitope (Figure 3C). After 6–8 h, maximal uptake was reached, correlating with a maximum of epitope presentation on the cell surface (Supplementary Figure S2).

The SiNP platform can be applied as carrier for various vaccine antigens

After demonstrating the ability of SiNPs to load and transport the model epitope SIINFEKL, we aimed at confirming the applicability of the SiNP platform in a clinically more relevant system, using the HPV16-derived HLA-A2-restricted epitope YMLDLQPET (E7/11–19). Previous studies have demonstrated that this epitope is surface-presented on HPV16-positive cervical cancer cells^{24,50} and is capable of inducing specific CD8⁺ T cell responses in MHC-humanized mice.³⁵ Furthermore, the application of YMLDLQPET-specific CD8⁺ T cells has already shown success in the clinic.⁵¹ To assess the uptake, processing, and surface presentation of the YMLDLQPET epitope linked to SiNPs *in vitro*, the human monocytic and HLA-A2-expressing cell line THP-1 was treated with SiNP-Arg~KKK-W-Cit-YMLDLQPET (Figure 4A) and was subsequently analyzed using mass spectrometry-based

solution with increasing peptide load, determined by DLS. (D-F) Flow cytometric analysis of surface presentation of SIINFEKL on H-2K^b molecules on DC2.4 cells. MFI = median fluorescence intensity. (D) Quantitative analysis and (E) representative histograms of SIINFEKL surface presentation upon treatment with indicated constructs. VSYNYFARL represents a negative control peptide. Statistical analysis was performed using unpaired two-tailed t tests. *****p* < 0.0001. (F) SIINFEKL surface presentation of indicated peptides, administered either as free peptides (gray) or attached to phosphorylated (blue) or arginylated (green) SiNPs. SLP represents the ovalbumin (OVA)-derived SIINFEKL-containing synthetic long peptide OVA24 (OVA/248–265A5K; DEVSGLEQLSEIINFEKLAAAAAK).

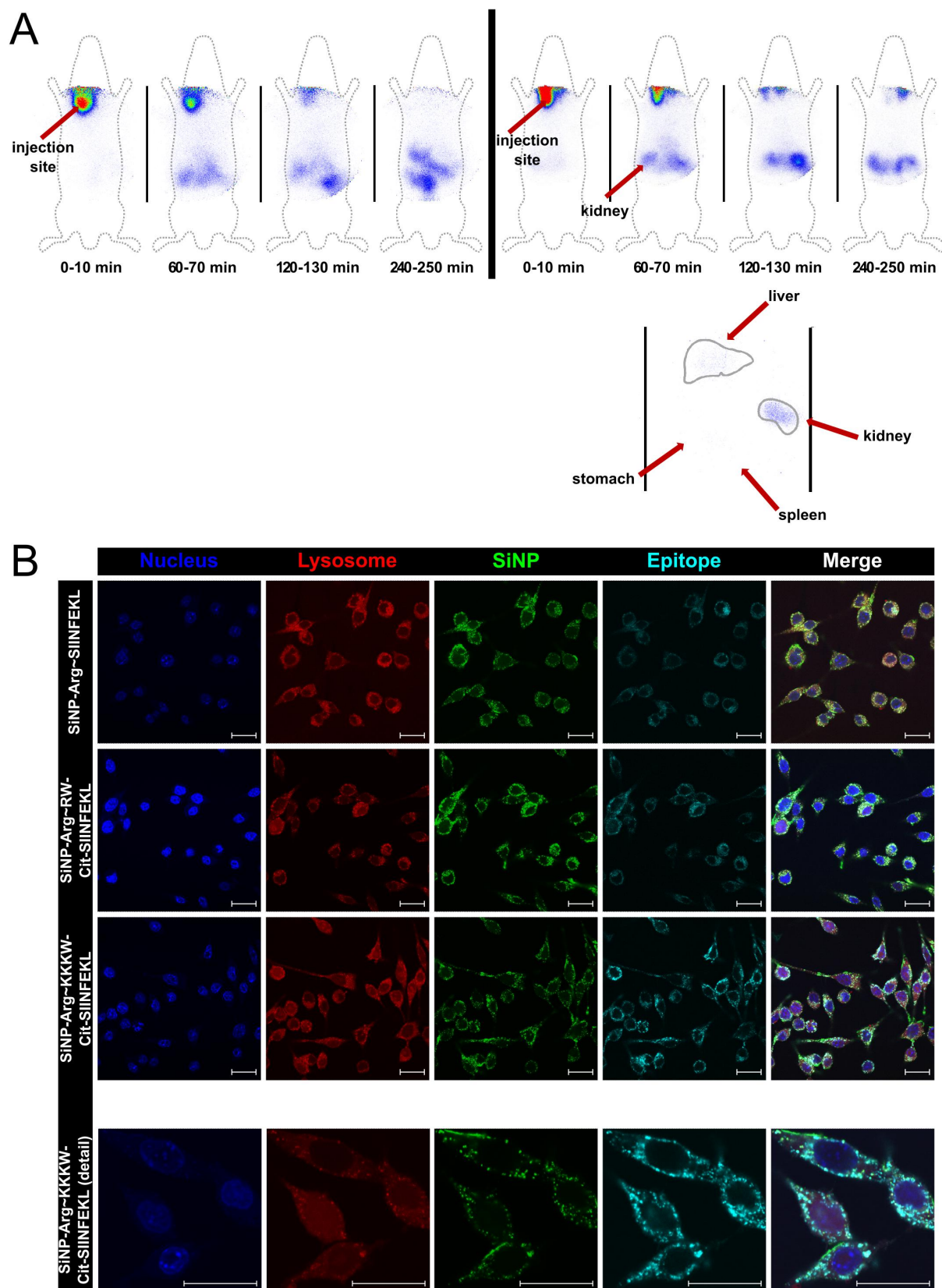


Figure 3. SiNP-epitope whole-body distribution and uptake by APCs. (A) Scintigraphic images displaying the *in vivo* whole-body distribution of free (left) and SiNP-bound isotope-labeled epitope (right) upon s.c. injection in Wistar rats ($n = 1/\text{condition}$) over time. Organs (right bottom) were analyzed 1 h after SiNP-bound epitope injection. (B-C) Confocal images of DC2.4 cells incubated with indicated fluorescently labeled SiNP-epitope constructs (SiNP-FITC (green), SIINFEKL-Cy5 (cyan)). After incubation, cells were stained with DAPI (blue) and lysotracker (red) for nucleus and lysosome detection, respectively. Scale bars, 20 μm . (B) Comparison of three constructs after 8 h incubation. (C) Monitoring of SiNP-Arg~KKKW-Cit-SIINFEKL-treated DC2.4 cells over the course of 8 h.

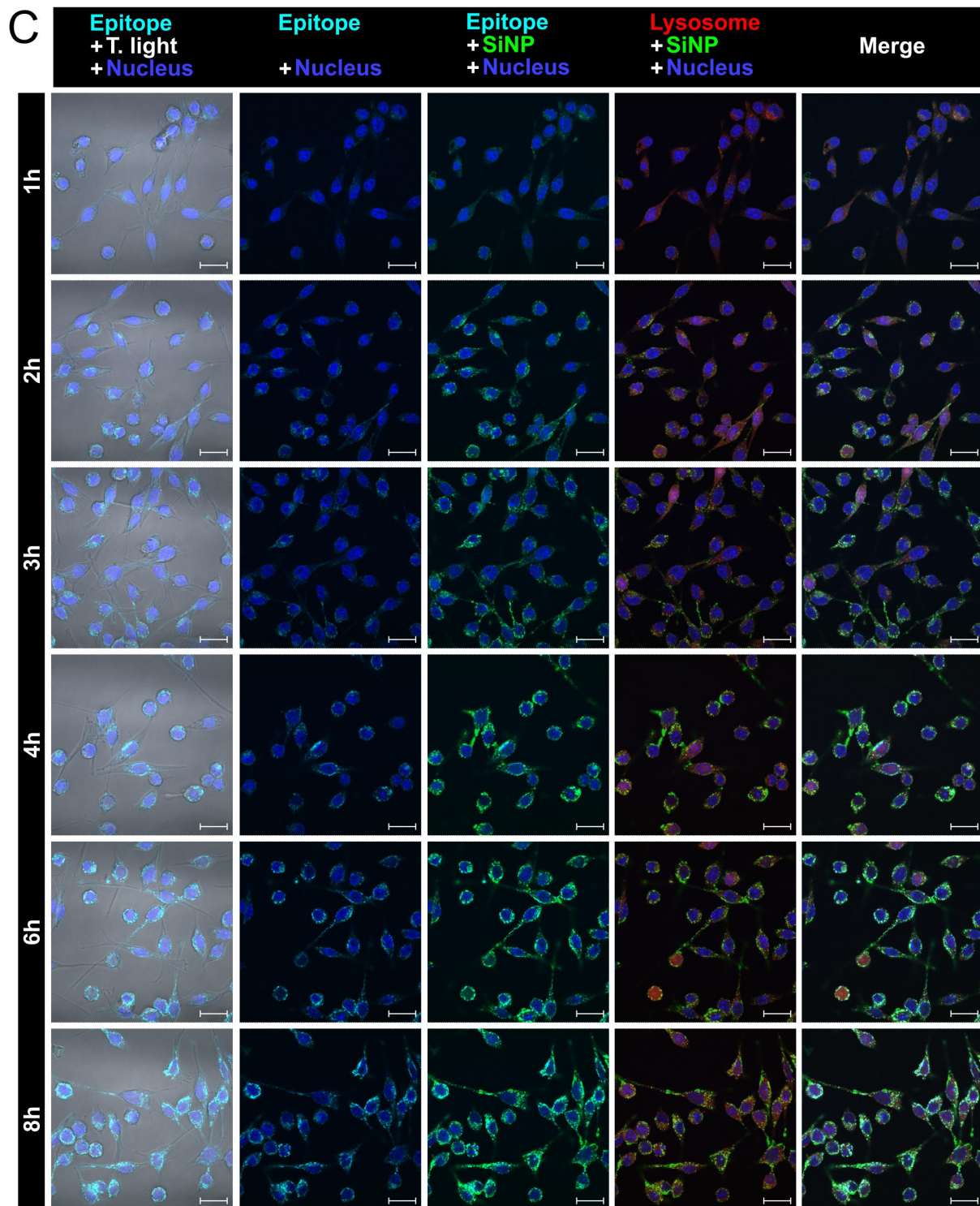


Figure 3. (Continued).

immuno-peptidomics. Analysis of epitopes extracted from HLA molecules confirmed successful surface presentation of YMLDLQPET on THP-1 cells upon treatment with epitope-loaded SiNPs, while untreated THP-1 cells did not present this epitope on their cell surface (Figure 4B,C), indicating that THP-1 cells successfully took up the SiNP constructs and were able to cleave off and present the HPV16 E7-derived epitope on their cell surface.

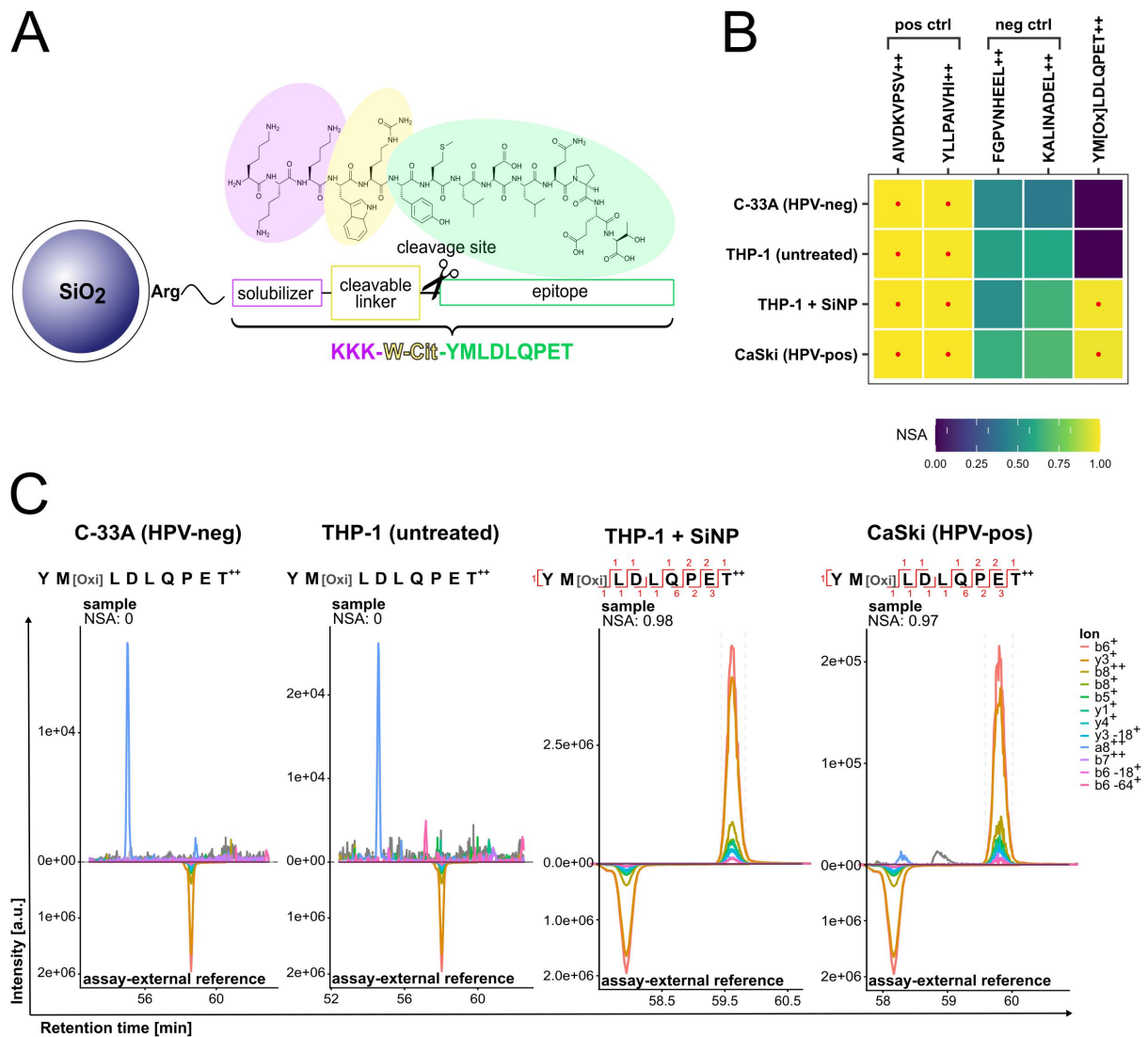


Figure 4. *In vitro* HLA-presentation of the HPV16 E7-derived epitope YMLDLQPET on a human APC cell line after incubation with epitope-loaded SiNPs. (A) Schematic representation of the SiNP construct including the clinically relevant epitope YMLDLQPET, derived from the HPV16 E7 oncoprotein. (B) Detection overview of different epitopes (columns) tested for surface presentation on different cell lines/treatments (rows). The color refers to the normalized spectral angle (NSA) as a measure of similarity between the acquired spectra for reference peptide and sample, and thus of the likelihood of detection. Red dots mark successful epitope detections. (C) Extracted ion chromatograms (XICs) for the epitope YMLDLQPET for each cell line/treatment tested, comparing the sample (top) with the corresponding stable isotope-labeled synthetic assay-external reference (bottom). Corresponding ion fragment patterns of both XICs indicate detection of YMLDLQPET on the cell line tested, red lettering indicates sequence coverage of the detected peptide.

Poly(I:C)-loaded SiNPs activate dendritic cell subsets capable of CD8⁺ T cell priming

While epitope presentation on MHC molecules represents the basic prerequisite for priming of a T cell response, the phenotype of the APCs and their expression of co-stimulatory molecules have a major impact on the fate of the T cell. We therefore assessed the effect of the different components of our therapeutic vaccine constructs – the epitope, the adjuvant poly(I:C) and SiNPs – alone as well as in different combinations *ex vivo* on conventional dendritic cells (cDCs) from spleens of C57BL/6 as well as A2.DR1 mice. While C57BL/6 mice express the murine MHC molecules H-2D^b, H-2K^b and I-A^b (Figure 5A) and can therefore bind and present the OVA-derived H-2K^b-restricted CD8⁺ T cell epitope SIINFEKL, A2.DR1 mice are MHC-humanized, i.e. they are knocked out for all murine MHC class-I and class-II alleles,⁴² and instead express HLA-DR1 and the HHD molecule, which comprises the α1 and α2 subunits of HLA-A*02:01

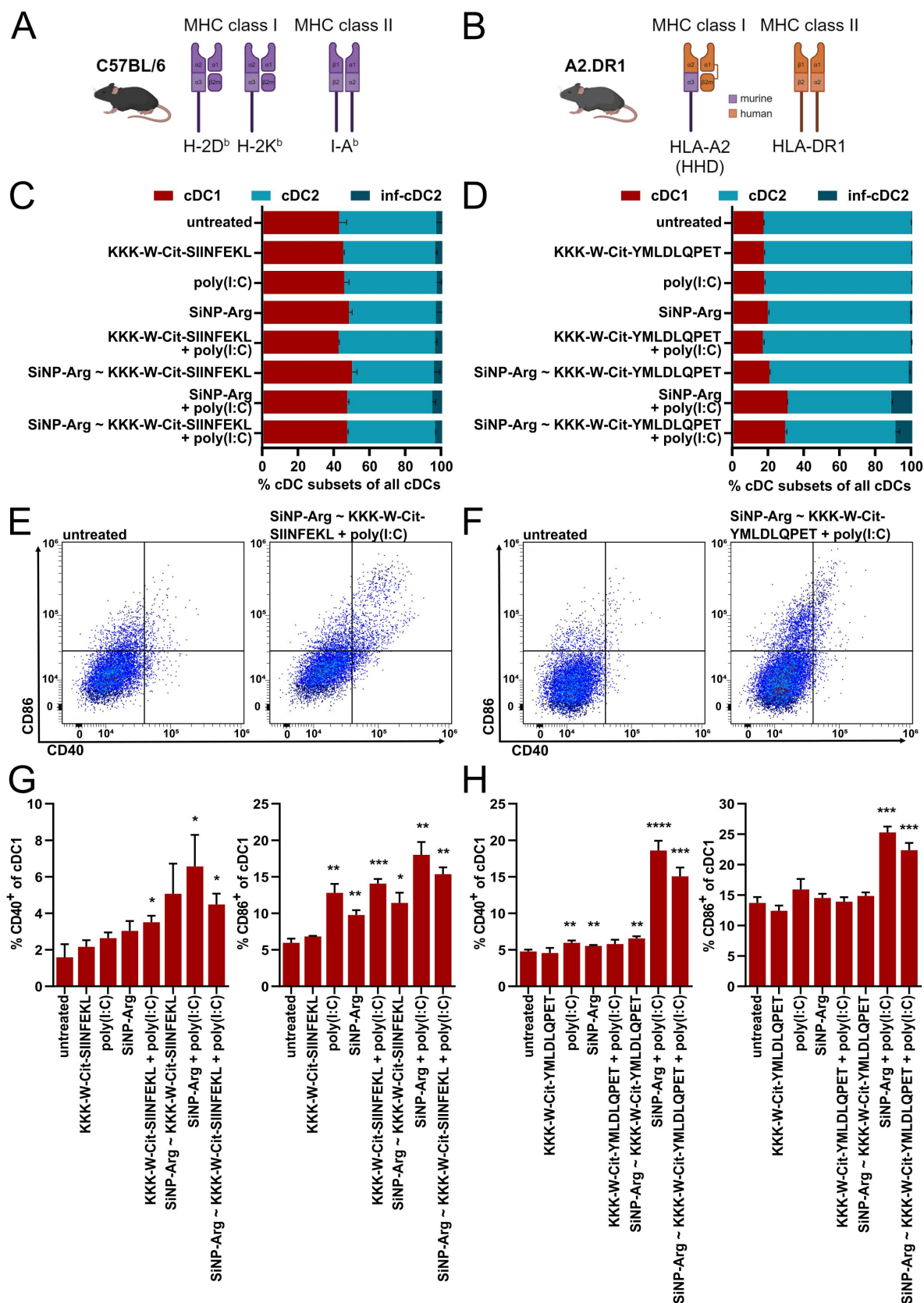


Figure 5. *Ex vivo* activation of conventional dendritic cells by SiNP constructs. (A) Schematic representation of the murine MHC molecules H-2D^b, H-2K^b and I-A^b expressed by C57BL/6 mice. (B) Schematic representation of the MHC molecules of A2.DR1 mice, expressing the HHD molecule (H-2D^b α 3 chain with HLA-A2 α 1 and α 2 chains, covalently linked to human β ₂m) and HLA-DR1. Splenocytes of the two mouse strains were incubated *ex vivo* with different constructs and subsequently

(Figure 5B).^{41,43,44} Thus, these mice can present HLA-A2- and HLA-DR1-restricted epitopes, such as the HPV16 E7-derived HLA-A2-restricted CD8⁺ T cell epitope YMLDLQPET.

The composition of the cDC compartment, consisting of cDC1, cDC2, and inflammatory cDC2 (inf-cDC2), was not markedly affected by any of the tested vaccine components and combinations when tested in C57BL/6-derived cells (Figure 5C). However, treatment of A2.DR1-derived cells with poly (I:C)-loaded SiNPs resulted in a distinct expansion of the cDC1 and inf-cDC2 subsets compared to untreated cells (Figure 5D), representing the two cDC subsets capable of cross-presentation and priming of CD8⁺ T cells.

Assessment of the activation markers CD40 and CD86, important co-stimulatory molecules for efficient T-cell priming, showed that treatment with poly (I:C) and SiNPs alone, but especially when used in combination, resulted in an expansion of CD40- and CD86-expressing cDC1 from both C57BL/6 (Figure 5E,G) and A2.DR1 mice (Figure 5F,H) compared to untreated cells. These results indicate activating as well as synergistic effects of these vaccine components, likely because SiNP coupling facilitates intracellular uptake of the TLR3 agonist poly(I:C). In contrast, incubation with the epitope alone did not affect the activation status of cDC1, emphasizing the necessity of administering the epitope in combination with a vaccine delivery system for proper DC targeting.

Similarly, poly(I:C)-loaded SiNPs (with and without the epitope) resulted in an expansion of CD40- and CD86-expressing cDC2 and inf-cDC2 (Supplementary Figure S3), which was particularly evident in A2.DR1-derived cells. However, while poly(I:C) alone already resulted in a slight increase in CD40- and CD86-positive cDC1, this effect was not observed in cDC2 and inf-cDC2. Instead, these cDC subsets were rather affected by the SiNPs, suggesting that the SiNPs themselves already provide adjuvant effects in these cell subsets.

SiNP vaccination induces epitope-specific cytotoxic CD8⁺ T cells

Next, we investigated whether different SiNP constructs were capable of inducing immune responses specific for the loaded epitope *in vivo*, using both the OVA as well as the HPV16 model systems.

First, C57BL/6 mice were vaccinated (Figure 6A) with free SIINFEKL or with SIINFEKL bound to 25 nm- or 40 nm-sized phosphorylated or arginylated SiNPs. As *ex vivo* combination treatment of DCs with SiNPs and the TLR3 agonist poly(I:C) had significantly increased the proportion of activated cDCs capable of CD8⁺ T cell priming (as demonstrated in Figure 5), and previous experiments had shown that addition of poly(I:C) as adjuvant was essential for induction of CD8⁺ T cell responses *in vivo* (data not shown), poly(I:C) was included in all vaccine formulations tested in this study. After three vaccinations, splenocytes from vaccinated mice were isolated and *in vitro* re-stimulated with SIINFEKL, and IFN γ production by CD8⁺ T cells was assessed through flow cytometry as a measure for the induction of an epitope-specific immune response (Figure 6B). Vaccination with SiNP-bound SIINFEKL resulted in the induction of approximately 0.5–1% epitope-specific CD8⁺ T cells among all splenic CD8⁺ T cells, while hardly any epitope-specific CD8⁺ T cells were detected upon administration of free SIINFEKL (Figure 6B,C). Comparison of different SiNP sizes and surface functionalizations did not show any significant differences, mirroring the *in vitro* data that demonstrated the equivalence of phosphorylation and arginylation for epitope binding. Also, administration of different epitope doses ranging from 12.5 to 50 nmol resulted in comparable epitope-specific CD8⁺ T cell frequencies (Supplementary Figure S4).

To confirm these results in a more clinically relevant model system, we used MHC-humanized A2.DR1 mice, presenting HLA-A2- and HLA-DR1-restricted epitopes. These mice were vaccinated with the HPV16 E7-derived HLA-A2-restricted epitope YMLDLQPET (Figure 6D). Also in this mouse model, we observed

analyzed via flow cytometry. (C-D) Ratio of cDC1, cDC2 and inf-cDC2 subsets among all cDCs in C57BL/6 (C) and A2.DR1 mice (D) upon incubation with indicated constructs. (E-F) Flow cytometry plots of indicated experimental groups showing CD40 and CD86 activation marker expression by the cDC1 subset in C57BL/6 (E) and A2.DR1 mice (F). (G-H) Quantitative analysis of CD40 (left) and CD86 (right) expression by cDC1s in C57BL/6 (G) and A2.DR1 mice (H) upon incubation with indicated constructs. Statistical analysis of the different experimental groups compared to the untreated control group was performed using unpaired two-tailed t tests. * $p < 0.05$, ** $p < 0.01$, *** $p < 0.001$, **** $p < 0.0001$.

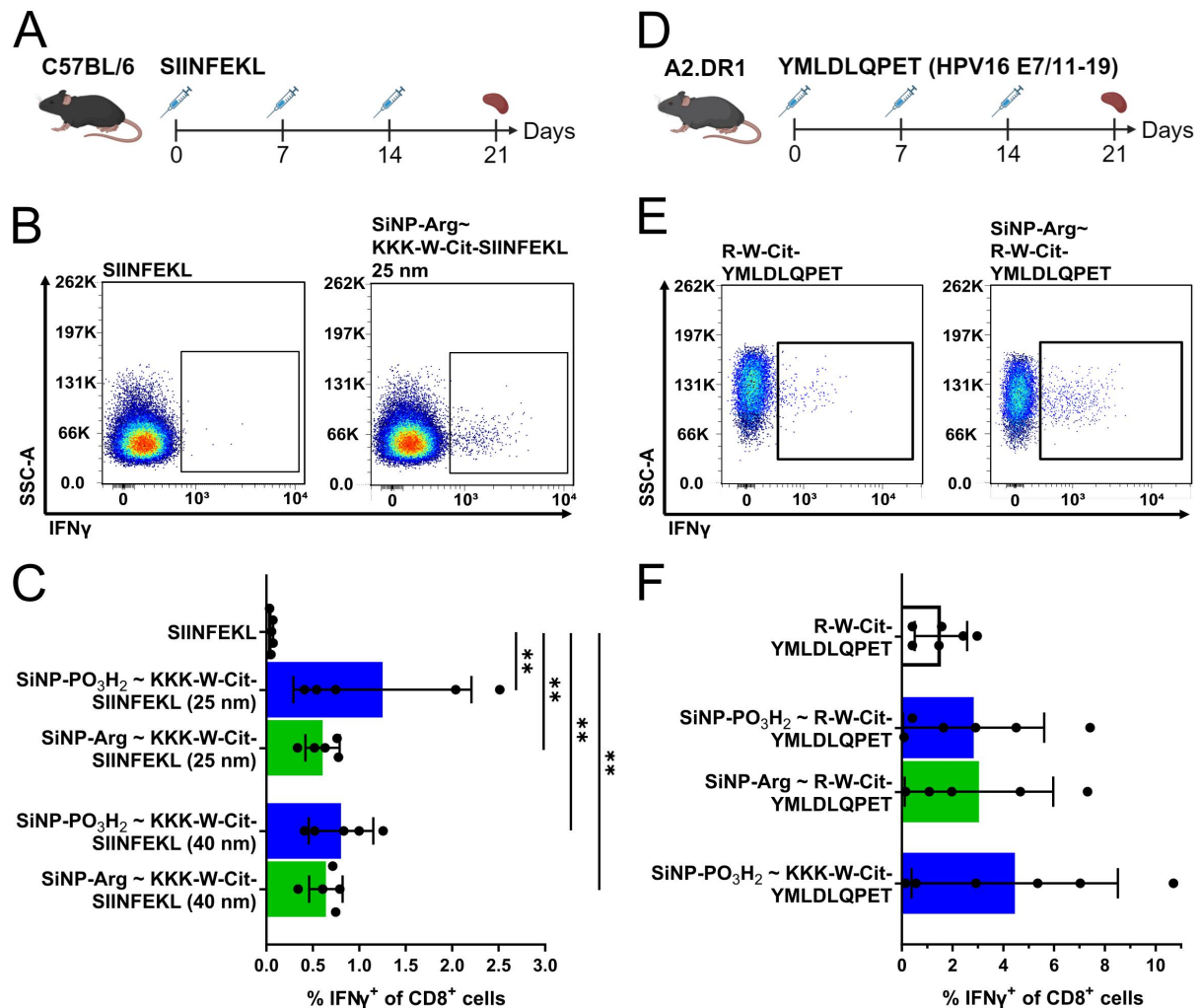


Figure 6. Induction of specific CD8 $^{+}$ T cells by SiNP constructs *in vivo*. (A) Schematic of the experimental setup. C57BL/6 mice were vaccinated three times s.c. on day 0, 7, and 14 with SIINFEKL-containing constructs including poly(I:C) as adjuvant. Splenocytes were isolated and analyzed on day 21. $n = 5$ mice/group. (B) Representative FACS plots showing IFN γ production of CD8 $^{+}$ T cells isolated from the spleen upon re-stimulation with SIINFEKL. (C) Quantitative analysis of IFN γ production of CD8 $^{+}$ T cells isolated from the spleens upon re-stimulation with SIINFEKL. Statistical analysis was performed using unpaired, two-tailed Mann-Whitney tests. $^{**}p < 0.01$. (D) Schematic of the experimental setup. A2.DR1 mice were vaccinated three times s.c. on day 0, 7, and 14 with YMLDLQPET (HPV16 E7/11-19)-containing constructs including poly(I:C) as adjuvant. Splenocytes were isolated and analyzed on day 21. $n = 6$ mice/group. (E) Representative FACS plots showing IFN γ production of CD8 $^{+}$ T cells isolated from the spleen upon re-stimulation with YMLDLQPET. (F) Quantitative analysis of IFN γ production of CD8 $^{+}$ T cells isolated from the spleens upon re-stimulation with YMLDLQPET.

a trend toward higher frequencies of epitope-specific CD8 $^{+}$ T cells when the epitope was attached to SiNPs, compared to free epitope (Figure 6E,F). As, again, results from using different surface functionalizations and/or solubilizers were highly similar, manufacturing reasons decided for arginylated SiNPs, with epitope attachment via the KKK-W-Cit solubilizer/linker combination as the final SiNP construct to be tested further.

Therapeutic vaccination with SiNP-YMLDLQPET constructs can eliminate HPV16 E6/E7-positive tumors

To assess if the observed SiNP-epitope vaccination-induced immune responses were capable of promoting tumor control, YMLDLQPET-loaded SiNPs were administered to A2.DR1 mice bearing tumors formed by the syngeneic HPV16 E6/E7-positive tumor cell line PAP-A2 (Figure 7A).³⁵ Immunopeptidomic analysis of

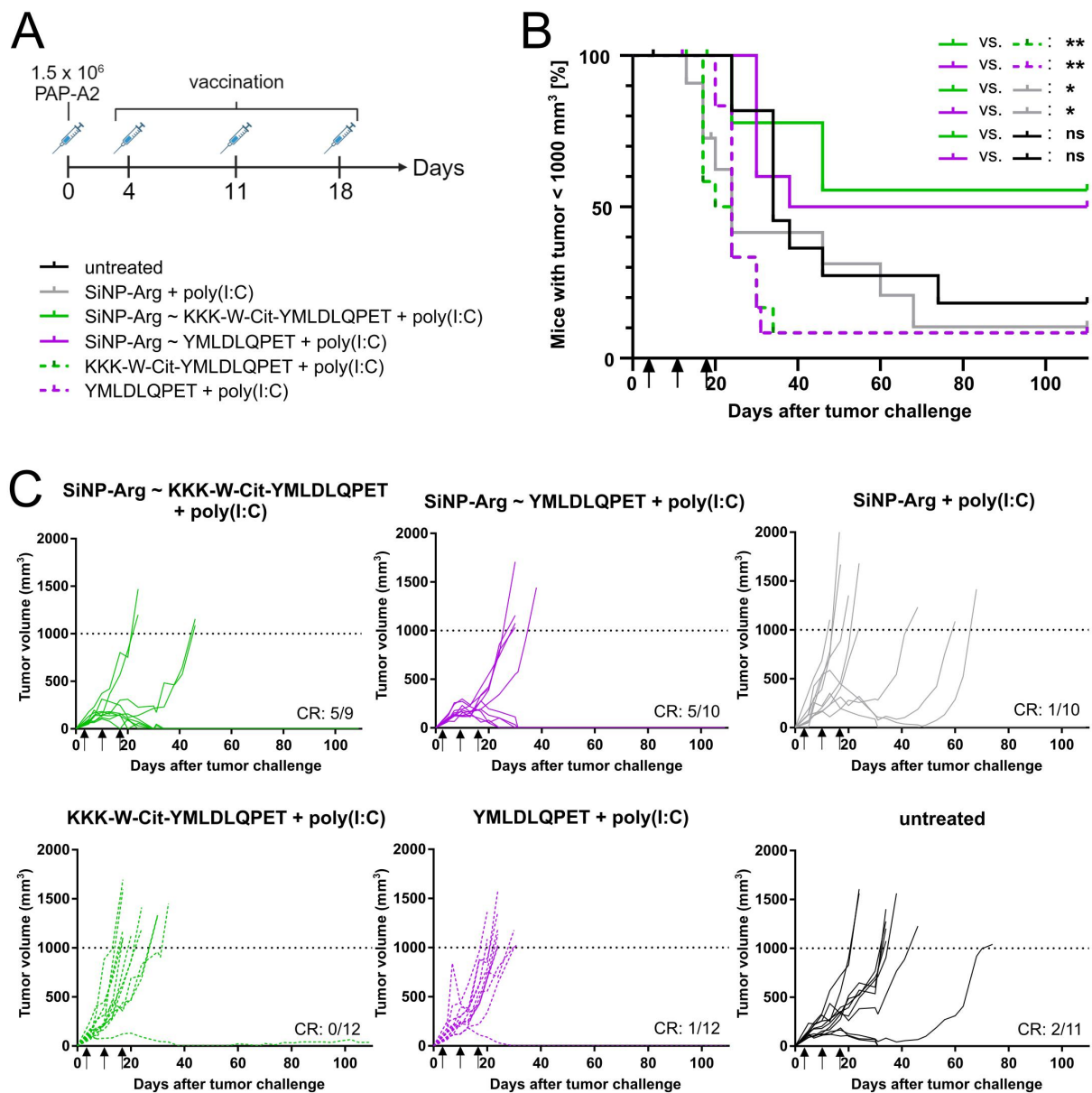


Figure 7. Therapeutic SiNP vaccination of A2.DR1 mice bearing HPV16 E6/E7-positive tumors. (A) Schematic of the experimental setup. A2.DR1 were injected s.c. with 1.5×10^6 HPV16 E6/E7-positive PAP-A2 tumor cells on day 0 ($n = 12$ /group) and vaccinated on day 4, 11, and 18 with indicated constructs. Tumor volume was monitored twice a week. (B) Cumulative survival curves of different treatment groups. Arrows indicate vaccination time points. Statistical analysis was performed using log-rank (Mantel Cox) test. * $p < 0.05$, ** $p < 0.01$. (C). Individual tumor growth curves of uncensored mice by treatment. CR = complete response.

PAP-A2 cells proved the surface presentation of the target epitope YMLDLQPET on HHD (Supplementary Figure S5), confirming the cells' principal susceptibility to immune attack by YMLDLQPET-specific CD8⁺ T cells. Vaccination of mice with free epitope (either with or without the solubilizer/linker KKK-W-Cit) resulted in survival rates of approximately 10%, similar to untreated mice or mice vaccinated with SiNPs loaded only with the adjuvant poly (I:C) (Figure 7B,C). In contrast, vaccination of tumor-bearing mice with the SiNP-Arg~KKK-W-Cit-YMLDLQPET and poly(I:C) formulation resulted in complete tumor regression (CR) in 5 out of 9 mice (overall survival rate of 55.6%), while vaccination with the SiNP construct without the solubilizer/linker led to CR in 5 out of 10 mice (overall survival rate of 50%) (Figure 7B,C). Compared to the respective relevant control groups, vaccinated with the respective free epitope and poly(I:

C), and compared to the group vaccinated with poly(I:C)-loaded SiNPs only, these effects were found to be statistically significant. Interestingly, comparison to the untreated group, while being clearly discernible, was not found to be statistically significant.

Discussion

Therapeutic cancer vaccinations work by eliciting cellular immune responses against antigens that are specific to the tumor. To this end, these antigens need to be administered in a way that ensures efficient uptake by APCs capable of activating CD8⁺ T cells. In the case of administering protein or peptide antigens, these APCs need to be capable of cross-presentation.⁵² To enhance antigen stability as well as uptake and presentation by APCs, various nanoparticle-based vaccine delivery systems are currently under investigation.⁷ Here, we present a novel nanoparticle-based vaccination platform that is suitable for various vaccine antigens. The platform is based on SiNPs, a material that provides several useful characteristics, such as a simple and cost-effective manufacturing process, stability at different conditions, and easily modifiable surfaces.^{18–20} For these reasons, SiNPs have already been widely used in the field of biomedicine, e.g. for drug delivery and biomedical imaging, as well as in other industries, such as advanced catalysis, environmental remediation, and water purification.⁵³

SiNPs are overall considered to be safe and exhibit good biocompatibility, which has been proven in numerous studies on cell lines, animals, and humans.⁵⁴ Nevertheless, several reports describe toxic effects of SiNPs *in vitro* and *in vivo*.¹⁸ Overall, it has been found that the toxicity strongly depends on different biochemical aspects of SiNPs, such as size, porosity, and surface chemistry.⁵⁴ In this study, we showed that uncoated SiNPs, displaying hydroxyl groups on their surface, were indeed highly cell-toxic when incubated with PBMCs. However, surface functionalization (in our case using arginylation) abrogated this toxic effect and made the SiNPs well tolerable even at high concentrations. A more detailed assessment of the *ex vivo* toxicity of SiNPs has already been performed.³³ Furthermore, regarding *in vivo* application, literature suggests that aqueous solutions and body fluids provide suitable conditions for amorphous SiNPs, as used in this study, to dissolve into silicic acid, which is excreted through the kidneys without accumulating in the body.^{55,56} These SiNPs therefore provide a good safety profile that is comparable to polymeric NPs which usually break down into by-products that are easily excreted from the body.⁵⁷ In contrast, lipid NPs (LNPs) – although selectively approved for clinical use – are criticized for their potential toxicities due to the incorporation of ionizable lipids, that can induce inflammation and liver toxicity, as well as PEGylated lipids, to which an antibody response can be provoked upon repeated dosing.^{58,59} LNPs therefore raise overall more safety concerns than amorphous SiNPs, emphasizing the SiNPs' suitability as therapeutic vaccine platform. Nevertheless, long-term assessment of *in vivo* biodistribution and toxicity of the SiNPs used in this study must be performed before this platform can be tested in humans.

While SiNPs can be generated in various sizes, studies have shown that the optimal particle size range for efficient entry into the lymphatic system as well as subsequent accumulation within lymph nodes lies between 10–100 nm, with particles at the lower end of this size range being particularly effective.^{47,48} This size promotes direct uptake of NPs by lymph node-resident DCs,^{60,61} representing the DC subpopulation most capable of cross-presenting the antigen for priming of CD8⁺ cytotoxic T cells.⁵² In comparison, smaller NPs rapidly exit the lymph nodes again into the bloodstream and are cleared from the body, while larger NPs show difficulties entering the lymphatic system at all and need to be actively transported by peripheral APCs.^{47,48} Based on this data, we decided to focus on SiNPs with diameters of 20–40 nm. Analysis of SiNP whole-body distribution suggested prolonged presence of SiNP-bound epitope at the injection site compared to free epitope, which would increase the chance of APC uptake and potentially facilitate a prolonged therapeutic effect. Unfortunately, it was not possible to visualize the presence of the SiNPs in the local lymph node due to the strong signal from the depot that formed at the injection site. Nevertheless, we further demonstrated induction of a CD8⁺ T cell response upon vaccination with SiNPs, indicating successful transport of the antigen to secondary lymphoid organs.

With the goal of providing a broadly applicable vaccine delivery platform, we evaluated different linker/solubilizer sequences that would allow the attachment as well as release and processing of various peptides, independent of their biochemical characteristics. The cleavable linker W-Cit was chosen based on the work of Dubowchik et al.⁶² This sequence is likely targeted by the lysosomal cysteine protease cathepsin B, which

prefers amino acids with a large hydrophobic side chain in the P2 site of the peptide,^{63,64} in our case provided by tryptophan. Peptide release and MHC loading worked well with this linker, as shown by flow cytometric, microscopic as well as immunopeptidomic analyses, where surface presentation of the W-Cit-linked epitopes consistently peaked within a few hours after start of the incubation. Our data further emphasize the importance of a careful design of the peptide sequence: While attachment of the linker to the N-terminus of the minimal epitope was well processable, C-terminal elongation of the minimal epitope as well as C-terminal placement of the linker reduced surface presentation of the target epitope dramatically. These findings are in line with other literature suggesting that particularly the C-terminus of the epitope needs to be precisely defined as it contains important anchor residues for stable binding to the MHC I peptide-binding groove,^{65,66} while the N-terminus can be trimmed later in the cytosol or endoplasmic reticulum by different peptidases if necessary.⁶⁷ The simplest way to ensure generation of the correct epitope that can bind and be presented by MHC I molecules is therefore to reduce the necessity of cell-intrinsic processing to an absolute minimum, as previously shown by placing an HPV epitope at the C-terminal position of a protein in a CMV-based vaccine.⁶⁸ We achieved this by directly using the minimal epitope, N-terminally connected to the SiNP through the W-Cit cleavable linker, producing considerably better results than using an SLP or whole protein sequence.

Apart from a cleavable linker, we further added a solubilizer sequence with the goal of increasing the water solubility of the attached peptide, allowing us to attach various peptides independent of their water solubility. Both sequences tested (KKK and R) consist of positively charged amino acids easily soluble in water. Addition of these amino acids therefore increases the total charge of the cargo peptide and consequently improves its water solubility, allowing for its attachment to SiNPs and preparation of an aqueous, DMSO-free solution for vaccination.

While the efficient cleavage and presentation of the epitope on MHC molecules on the APC's surface represents the basic prerequisite for priming of a T cell response, provision of further co-stimulatory signals is necessary for proper T cell activation.⁶⁹ Furthermore, the type of APC presenting the epitope can have a major impact on the fate of the activated T cell. The most prominent APC types involved in anti-tumor immunity are the cDC1 and inf-cDC2 subsets, both capable of cross-presenting antigens for priming of CD8⁺ T cells.⁷⁰ Here, we showed that *ex vivo* treatment of splenocytes with our therapeutic vaccine construct, containing a CD8⁺ T cell epitope and the adjuvant poly(I:C) bound to SiNPs, resulted in the expansion and activation of exactly these cDC subsets. Interestingly, this effect was more pronounced in the A2.DR1 mouse strain, despite the common C57BL/6 background.

Finally, our *in vivo* studies, both in the OVA and the HPV model system, demonstrated that administration of the respective epitopes bound to SiNPs induced epitope-specific CD8⁺ T cell responses in the spleen. In the HPV setting, we also observed distinct anti-tumor effects. The HPV tumor model that we chose for our studies is based on PAP-A2 cells, which express the viral oncoproteins HPV16 E6 and E7 and are syngeneic to the A2.DR1 mouse strain, which expresses HLA-A2 and HLA-DR1.³⁵ This allows testing of the HLA-A2-restricted HPV16 E7-derived epitope YMLDLQPET, a clinically highly relevant epitope, as administration of TCR-engineered T cells against it has already shown success in the clinic.⁵¹ While the chosen tumor model allows us to evaluate clinically relevant HLA-A2-restricted epitopes, which cannot be assessed by typically used fully murine HPV tumor models such as TC-1,⁷¹ epitopes restricted to other HLA supertypes cannot be tested in this mouse strain. Furthermore, the PAP-A2 tumor model is characterized by its aggressive tumor growth, making it challenging to achieve a high cure rate. Even when using the highly immunogenic amph-peptide vaccine platform, initially developed by Liu et al.,⁷² a cure rate of maximum 50% was observed in a previous study using PAP-A2 tumor-bearing A2.DR1 mice.³⁵ Using SiNPs, we here observed cure rates of 50–55%, demonstrating their comparability to the amph-peptide vaccine format in the PAP-A2 tumor model and overall stressing the effectivity of the SiNP vaccine platform. Despite these promising results, this study was limited to only one single minimal epitope (for each model system) as a proof of concept. A therapeutic vaccine containing only a single MHC I-binding epitope is, however, unlikely to achieve long-term therapeutic benefits due to immune evasion mechanisms, such as loss of heterozygosity of HLA-I alleles, and lack of CD4⁺ T cell help.^{73,74} Future studies should therefore focus on the suitability of SiNPs to load a set of MHC I- as well as MHC II-binding epitopes covering all major HLA supertypes, thereby creating a universally applicable vaccine. In addition, long-term immunogenicity as well as direct comparison to other vaccine platforms that are currently developed need to be assessed to fully

determine the potency of the SiNP platform as a therapeutic cancer vaccine. It is difficult to assess such differences from the available literature, as many factors extrinsic to the vaccine platform (such as physicochemical nature of the antigen, adjuvant, and importantly timing and number of booster immunizations) affect immune response durability.⁵

As no anti-tumor effects were observed in the groups receiving the respective antigen without SiNPs, our results emphasize the importance of a carrier system that facilitates safe transport of the vaccine to secondary lymphoid organs, improved uptake by APCs, and a prolonged therapeutic effect through reduction of the clearance rate. While the SiNP platform is designed to be used for a broad spectrum of indications, our specific interest lies in the treatment of HPV-mediated malignancies. While this study confirmed the applicability of the SiNP platform for induction of systemic HPV16-directed cytotoxic T cell responses, it is important to consider that HPV naturally infects mucosal tissues in the anogenital and head and neck region.⁷⁵ Future studies therefore need to focus on evaluating the suitability of SiNPs for induction of local immune responses at sites of natural infection. A number of therapeutic HPV16 vaccines are currently evaluated in clinical studies, but so far have shown only moderate efficacies.^{76,77} In most cases, the vaccines contained the whole (mutated) E7 protein sequence in the form of peptide or nucleic acids, either administered directly or incorporated into carrier systems, such as lipid nanoparticles or viral vectors.^{1,77,78} These vaccine formulations often necessitate cold chain storage and delivery, which is difficult to provide especially in low-income countries, where the prevalence of HPV-mediated cancer is highest and a therapeutic vaccine consequently most needed.²⁵ SiNPs are known for their stability at different temperatures, which we also confirmed in our own lab (data not shown). The presented vaccine platform may therefore provide a solution to these transport and storage challenges and could contribute to a therapeutic HPV vaccine with worldwide applicability, as set forward in the recently published preferred product characteristics (PPCs) for therapeutic HPV vaccines by the WHO.⁷⁹

In conclusion, the presented SiNP vaccine delivery platform represents a safe, versatile, easy to produce and efficacious tool that holds great promise as a vaccine carrier for treatment of a variety of infectious and cancerous diseases, including HPV-associated malignancies.

Acknowledgments

We thank the Institut Pasteur for providing the A2.DR1 mouse strain. We gratefully acknowledge the DKFZ Flow Cytometry Core Facility (CFFC), the DKFZ Proteomics Core Facility, the DKFZ Light Microscopy Facility (LMF) as well as the DKFZ biostatistics department for their technical and statistical support. Furthermore, we want to thank Alexandra Klevenz and Rebecca Köhler for their excellent technical assistance, and Dr. Jonas Becker and Kim van der Gouw, MSc, for their contributions to figure design.

All particles and their physicochemical characterization were provided by the Silvacx team, the SiNP toxicity data were provided by the DZNE team. Epitope presentation, microscopy, immunopeptidomics, DC characterization and A2.DR1 *in vivo* work was performed by the DKFZ team. C57BL/6 *in vivo* work was performed at a CRO appointed by Silvacx, analysis was performed at DKFZ. *In vivo* distribution experiments in rats were contributed by Heidelberg University. All authors have read and approved the final version of this manuscript.

Author contributions

CRediT: **Sebastian Kruse:** Conceptualization, Formal analysis, Investigation, Validation, Visualization, Writing – original draft, Writing – review & editing; **Lia T. Fricke:** Formal analysis, Investigation, Validation, Visualization, Writing – review & editing; **Samantha Zottnick:** Formal analysis, Validation, Visualization, Writing – original draft, Writing – review & editing; **Ann-Katrin Schlosser:** Formal analysis, Investigation, Validation, Visualization, Writing – original draft, Writing – review & editing; **Agnieszka K. Grabowska:** Project administration, Supervision, Validation, Visualization, Writing – review & editing; **Eva Feidt:** Investigation, Validation, Visualization, Writing – review & editing; **Philipp Uhl:** Investigation, Validation, Visualization, Writing – review & editing; **Ellen Junglas:** Investigation, Validation, Visualization, Writing – review & editing; **Jonas D. Förster:** Formal analysis, Investigation, Validation, Visualization, Writing – review & editing; **Josephine Blersch:** Formal analysis, Investigation, Validation, Visualization, Writing – review & editing; **Philip Denner:** Formal analysis, Investigation, Validation, Writing – review & editing; **Manina Günter:** Investigation, Writing – review & editing; **Stella E. Autenrieth:** Formal analysis, Resources, Supervision, Validation, Writing – review & editing; **Eugenio Fava:** Resources, Supervision, Writing – review & editing; **Walter Mier:** Resources, Supervision, Writing – review & editing; **Armin Kübelbeck:** Conceptualization,

Funding acquisition, Investigation, Project administration, Resources, Supervision, Validation, Visualization, Writing – review & editing; **Angelika B. Riemer**: Conceptualization, Funding acquisition, Project administration, Resources, Supervision, Validation, Writing – original draft, Writing – review & editing.














Disclosure statement

AK is a co-inventor on a patent related to this study (Patent family WO 2010/006753). SK, AKG, EFe, EJ, AK, and ABR are inventors on patent applications related to this study (EP20174156.8, EP20196027.5, EP20196024.2). ABR received consulting fees from Life Science Inkubator GmbH for an unrelated project during the conduct of this study. AK is founder and has an ownership interest in Silvax Pharmaceutical Exploration and Research GmbH. All other authors report no conflict of interest.

Funding

SZ and A-KS were funded by PhD scholarships from the Helmholtz International Graduate School of the German Cancer Research Center (DKFZ). LTF was funded by MD scholarships from the German Cancer Aid and the German Center for Infection Research (DZIF). This research was partly supported by the Ministry of Innovation, Science and Research of the State of North Rhine-Westphalia [Grand number FKZ-005-1704-0011] via a collaboration research agreement between the Life Science Inkubator GmbH and the DKFZ.

ORCID

Sebastian Kruse  <http://orcid.org/0000-0002-4028-1391>
 Lia T. Fricke  <http://orcid.org/0009-0002-9985-4227>
 Samantha Zottnick  <http://orcid.org/0000-0002-9077-635X>
 Ann-Katrin Schlosser  <http://orcid.org/0000-0003-1269-2537>
 Philipp Uhl  <http://orcid.org/0000-0002-8616-5599>
 Jonas D. Förster  <http://orcid.org/0000-0003-3437-6738>
 Josephine Blersch  <http://orcid.org/0000-0003-0637-3273>
 Philip Denner  <http://orcid.org/0000-0002-4301-5013>
 Manina Günter  <http://orcid.org/0009-0002-5616-2589>
 Stella E. Autenrieth  <http://orcid.org/0000-0003-4054-9041>
 Eugenio Fava  <http://orcid.org/0000-0002-3737-0334>
 Walter Mier  <http://orcid.org/0000-0002-3901-5061>
 Angelika B. Riemer  <http://orcid.org/0000-0002-5865-0714>

Data availability statement

The data that support the findings of this study are available from the corresponding author, ABR, upon reasonable request.

References

1. Saxena M, van der Burg SH, Melief CJM, Bhardwaj N. Therapeutic cancer vaccines. *Nat Rev Cancer*. 2021;21(6):360–378. doi: [10.1038/s41568-021-00346-0](https://doi.org/10.1038/s41568-021-00346-0).
2. Embgenbroich M, Burgdorf S. Current concepts of antigen cross-presentation. *Front Immunol*. 2018;9:1643. doi: [10.3389/fimmu.2018.01643](https://doi.org/10.3389/fimmu.2018.01643).
3. Facciola A, Visalli G, Laganà A, Di Pietro A. An overview of vaccine adjuvants: current evidence and future perspectives. *Vaccines (Basel)*. 2022;10(5):819. doi: [10.3390/vaccines10050819](https://doi.org/10.3390/vaccines10050819).
4. Ulmer JB, Wahren B, Liu MA. Gene-based vaccines: recent technical and clinical advances. *Trends Mol Med*. 2006;12(5):216–222. doi: [10.1016/j.molmed.2006.03.007](https://doi.org/10.1016/j.molmed.2006.03.007).
5. Fan T, Zhang M, Yang J, Zhu Z, Cao W, Dong C. Therapeutic cancer vaccines: advancements, challenges, and prospects. *Sig Transduct Target Ther*. 2023;8(1):450. doi: [10.1038/s41392-023-01674-3](https://doi.org/10.1038/s41392-023-01674-3).
6. Vert M, Doi Y, Hellwich K-H, Hess M, Hodge P, Kubisa P, Rinaudo M, Schué F. Terminology for biorelated polymers and applications (IUPAC recommendations 2012). *Pure Appl Chem*. 2012;84(2):377–410. doi: [10.1351/PAC-REC-10-12-04](https://doi.org/10.1351/PAC-REC-10-12-04).
7. Mitchell MJ, Billingsley MM, Haley RM, Wechsler ME, Peppas NA, Langer R. Engineering precision nanoparticles for drug delivery. *Nat Rev Drug Discov*. 2021;20(2):101–124. doi: [10.1038/s41573-020-0090-8](https://doi.org/10.1038/s41573-020-0090-8).

8. Kuai R, Ochyl LJ, Bahjat KS, Schwendeman A, Moon JJ. Designer vaccine nanodiscs for personalized cancer immunotherapy. *Nat Mater.* 2017;16(4):489–496. doi: [10.1038/nmat4822](https://doi.org/10.1038/nmat4822).
9. Yu X, Dai Y, Zhao Y, Qi S, Liu L, Lu L, Luo Q, Zhang Z. Melittin-lipid nanoparticles target to lymph nodes and elicit a systemic anti-tumor immune response. *Nat Commun.* 2020;11(1):1110. doi: [10.1038/s41467-020-14906-9](https://doi.org/10.1038/s41467-020-14906-9).
10. Kranz LM, Diken M, Haas H, Kreiter S, Loquai C, Reuter KC, Meng M, Fritz D, Vascotto F, Hefesha H, et al. Systemic RNA delivery to dendritic cells exploits antiviral defence for cancer immunotherapy. *Nature.* 2016;534(7607):396–401. doi: [10.1038/nature18300](https://doi.org/10.1038/nature18300).
11. Persano S, Guevara ML, Li Z, Mai J, Ferrari M, Pompa PP, Shen H. Lipopolyplex potentiates anti-tumor immunity of mRNA-based vaccination. *Biomaterials.* 2017;125:81–89. doi: [10.1016/j.biomaterials.2017.02.019](https://doi.org/10.1016/j.biomaterials.2017.02.019).
12. Moynihan KD, Opel CF, Szeto GL, Tzeng A, Zhu EF, Engreitz JM, Williams RT, Rakhra K, Zhang MH, Rothschilds AM, et al. Eradication of large established tumors in mice by combination immunotherapy that engages innate and adaptive immune responses. *Nat Med.* 2016;22(12):1402–1410. doi: [10.1038/nm.4200](https://doi.org/10.1038/nm.4200).
13. van der Maaden K, Heuts J, Camps M, Pontier M, Terwisscha van Scheltinga A, Jiskoot W, Ossendorp F, Bouwstra J. Hollow microneedle-mediated micro-injections of a liposomal HPV E743–63 synthetic long peptide vaccine for efficient induction of cytotoxic and T-helper responses. *J Control Release.* 2018;269:347–354. doi: [10.1016/j.jconrel.2017.11.035](https://doi.org/10.1016/j.jconrel.2017.11.035).
14. Chu Y, Qian L, Ke Y, Feng X, Chen X, Liu F, Yu L, Zhang L, Tao Y, Xu R, et al. Lymph node-targeted neoantigen nanovaccines potentiate anti-tumor immune responses of post-surgical melanoma. *J Nanobiotechnol.* 2022;20(1):190. doi: [10.1186/s12951-022-01397-7](https://doi.org/10.1186/s12951-022-01397-7).
15. Loquai C, Hassel JC, Oehm P, Derhovanessian E, Jabulowsky RA, Gold M, Schwarck-Kokarakis D, Attig S, Cuk K, Vogler I, et al. A shared tumor-antigen RNA-lipoplex vaccine with/without anti-PD1 in patients with checkpoint-inhibition experienced melanoma. *J Clin Oncol.* 2020;38(15_suppl):3136–3136. doi: [10.1200/JCO.2020.38.15_suppl.3136](https://doi.org/10.1200/JCO.2020.38.15_suppl.3136).
16. Rojas LA, Sethna Z, Soares KC, Olcese C, Pang N, Patterson E, Lihm J, Ceglia N, Guasp P, Chu A, et al. Personalized RNA neoantigen vaccines stimulate T cells in pancreatic cancer. *Nature.* 2023;618(7963):144–150. doi: [10.1038/s41586-023-06063-y](https://doi.org/10.1038/s41586-023-06063-y).
17. Anselmo AC, Mitragotri S. Nanoparticles in the clinic: an update post COVID-19 vaccines. *Bioeng Transl Med.* 2021;6(3):e10246. doi: [10.1002/btm2.10246](https://doi.org/10.1002/btm2.10246).
18. Li Z, Mu Y, Peng C, Lavin MF, Shao H, Du Z. Understanding the mechanisms of silica nanoparticles for nanomedicine. *Wiley Interdiscip Rev Nanomed Nanobiotechnol.* 2021;13(1):e1658. doi: [10.1002/wnan.1658](https://doi.org/10.1002/wnan.1658).
19. Huang Y, Li P, Zhao R, Zhao L, Liu J, Peng S, Fu X, Wang X, Luo R, Wang R, et al. Silica nanoparticles: biomedical applications and toxicity. *Biomed Pharmacother.* 2022;151:113053. doi: [10.1016/j.biopha.2022.113053](https://doi.org/10.1016/j.biopha.2022.113053).
20. Choi Y, Kim J, Yu S, Hong S. pH- and temperature-responsive radially porous silica nanoparticles with high-capacity drug loading for controlled drug delivery. *Nanotechnology.* 2020;31(33):335103. doi: [10.1088/1361-6528/ab9043](https://doi.org/10.1088/1361-6528/ab9043).
21. Escriche-Navarro B, Escudero A, Lucena-Sánchez E, Sancenón F, García-Fernández A, Martínez-Máñez R. Mesoporous silica materials as an emerging tool for cancer immunotherapy. *Adv Sci.* 2022;9(26):2200756. doi: [10.1002/advs.202200756](https://doi.org/10.1002/advs.202200756).
22. International Agency for Research on Cancer. Agents classified by the IARC monographs, volumes 1–136 (update September 2024). [cited 2024 11 24]; <https://monographs.iarc.who.int/list-of-classifications>.
23. Pal A, Kundu R. Human papillomavirus E6 and E7: the cervical cancer hallmarks and targets for therapy. *Front Microbiol.* 2019;10:3116. doi: [10.3389/fmicb.2019.03116](https://doi.org/10.3389/fmicb.2019.03116).
24. Riemer AB, Keskin DB, Zhang G, Handley M, Anderson KS, Brusic V, Reinhold B, Reinherz EL. A conserved E7-derived cytotoxic T lymphocyte epitope expressed on human papillomavirus 16-transformed HLA-A2+ epithelial cancers. *J Biol Chem.* 2010;285(38):29608–29622. doi: [10.1074/jbc.M110.126722](https://doi.org/10.1074/jbc.M110.126722).
25. World Health Organization. Fact sheet: Human papillomavirus and cancer. [2024 11 24]; <https://www.who.int/news-room/fact-sheets/detail/human-papilloma-virus-and-cancer#:~:text=HPV>.
26. Sung H, Ferlay J, Siegel RL, Laversanne M, Soerjomataram I, Jemal A, Bray F. Global cancer statistics 2020: GLOBOCAN estimates of incidence and mortality worldwide for 36 cancers in 185 countries. *CA Cancer J Clin.* 2021;71(3):209–249. doi: [10.3322/caac.21660](https://doi.org/10.3322/caac.21660).
27. de Sanjose S, Quint WG, Alemany L, Geraets DT, Klaustermeier JE, Lloveras B, Tous S, Felix A, Bravo LE, Shin H-R, et al. Human papillomavirus genotype attribution in invasive cervical cancer: a retrospective cross-sectional worldwide study. *Lancet Oncol.* 2010;11(11):1048–1056. doi: [10.1016/S1470-2045\(10\)70230-8](https://doi.org/10.1016/S1470-2045(10)70230-8).
28. Lechner M, Liu J, Masterson L, Fenton TR. HPV-associated oropharyngeal cancer: epidemiology, molecular biology and clinical management. *Nat Rev Clin Oncol.* 2022;19(5):306–327. doi: [10.1038/s41571-022-00603-7](https://doi.org/10.1038/s41571-022-00603-7).
29. World Health Organization. Fact sheet: Immunization coverage. [2024 11 24]; <https://www.who.int/news-room/fact-sheets/detail/immunization-coverage>.
30. Berman TA, Schiller JT. Human papillomavirus in cervical cancer and oropharyngeal cancer: one cause, two diseases. *Cancer.* 2017;123(12):2219–2229. doi: [10.1002/cncr.30588](https://doi.org/10.1002/cncr.30588).
31. Lee MY, Allen CT. Immunotherapy for HPV malignancies. *Semin Radiat Oncol.* 2021;31(4):361–370. doi: [10.1016/j.semradonc.2021.02.008](https://doi.org/10.1016/j.semradonc.2021.02.008).

32. Stöber W, Fink A, Bohn E. Controlled growth of monodisperse silica spheres in the micron size range. *J Colloid and Interface Sci.* **1968**;26(1):62–69. doi: [10.1016/0021-9797\(68\)90272-5](https://doi.org/10.1016/0021-9797(68)90272-5).
33. Blersch J, Kurkowsky B, Meyer-Berhorn A, Grabowska AK, Feidt E, Junglas E, Roth W, Stappert D, Kübelbeck A, Denner P, Fava E. An ex vivo human model for safety assessment of immunotoxicity of engineered nanomaterials. *bioRxiv.* **2023**. doi:[10.1101/2023.06.29.547008](https://doi.org/10.1101/2023.06.29.547008).
34. Shen ZH, Reznikoff G, Dranoff G, Rock KL. Cloned dendritic cells can present exogenous antigens on both MHC class I and class II molecules. *J Immunol.* **1997**;158(6):2723–2730. doi: [10.4049/jimmunol.158.6.2723](https://doi.org/10.4049/jimmunol.158.6.2723).
35. Kruse S, Büchler M, Uhl P, Sauter M, Scherer P, Lan TCT, Zottnick S, Klevenz A, Yang R, Rösl F, et al. Therapeutic vaccination using minimal HPV16 epitopes in a novel MHC-humanized murine HPV tumor model. *Oncoimmunology.* **2018**;8(1):e1524694. doi: [10.1080/2162402X.2018.1524694](https://doi.org/10.1080/2162402X.2018.1524694).
36. Chong C, Marino F, Pak H, Racle J, Daniel RT, Müller M, Gfeller D, Coukos G, Bassani-Sternberg M. High-throughput and sensitive immunopeptidomics platform reveals profound interferon- γ -mediated remodeling of the human leukocyte antigen (HLA) ligandome. *Mol Cell Proteomics.* **2018**;17(3):533–548. doi: [10.1074/mcp.TIR117.000383](https://doi.org/10.1074/mcp.TIR117.000383).
37. Salek M, Förster JD, Becker JP, Meyer M, Charoentong P, Lyu Y, Lindner K, Lotsch C, Volkmar M, Momburg F, et al. OptiPRM: a targeted immunopeptidomics LC-MS workflow with ultra-high sensitivity for the detection of mutation-derived tumor neoepitopes from limited input material. *Mol Cell Proteomics.* **2024**;23(9):100825. doi: [10.1016/j.mcpro.2024.100825](https://doi.org/10.1016/j.mcpro.2024.100825).
38. MacLean B, Tomazela DM, Shulman N, Chambers M, Finney GL, Frewen B, Kern R, Tabb DL, Liebler DC, MacCoss MJ. Skyline: an open source document editor for creating and analyzing targeted proteomics experiments. *Bioinformatics.* **2010**;26(7):966–968. doi: [10.1093/bioinformatics/btq054](https://doi.org/10.1093/bioinformatics/btq054).
39. Toprak UH, Gillet LC, Maiolica A, Navarro P, Leitner A, Aebersold R. Conserved peptide fragmentation as a benchmarking tool for mass spectrometers and a discriminating feature for targeted proteomics. *Mol Cell Proteomics.* **2014**;13(8):2056–2071. doi: [10.1074/mcp.O113.036475](https://doi.org/10.1074/mcp.O113.036475).
40. R Core Team. R: a language and environment for statistical computing. Vienna, Austria: Foundation for Statistical Computing; **2013**.
41. Pascolo S, Bervas N, Ure JM, Smith AG, Lemonnier FA, Pérarnau B. Hla-a2.1-restricted education and cytolytic activity of CD8(+) T lymphocytes from beta2 microglobulin (beta2m) HLA-A2.1 monochain transgenic H-2Db beta2m double knockout mice. *J Exp Med.* **1997**;185(12):2043–2051. doi: [10.1084/jem.185.12.2043](https://doi.org/10.1084/jem.185.12.2043).
42. Madsen L, Labrecque N, Engberg J, Dierich A, Svejgaard A, Benoist C, Mathis D, Fugger L. Mice lacking all conventional MHC class II genes. *Proc Natl Acad Sci USA.* **1999**;96(18):10338–10343. doi: [10.1073/pnas.96.18.10338](https://doi.org/10.1073/pnas.96.18.10338).
43. Pajot A, Michel M-L, Fazilleau N, Pancré V, Auriault C, Ojcius D, Lemonnier FA, Lone Y-C. A mouse model of human adaptive immune functions: HLA-A2.1-/HLA-DR1-transgenic H-2 class I-/class II-knockout mice. *Eur J Immunol.* **2004**;34(11):3060–3069. doi: [10.1002/eji.200425463](https://doi.org/10.1002/eji.200425463).
44. Mathieu MG, Knights AJ, Pawelec G, Riley CL, Wernet D, Lemonnier FA, Straten PT, Mueller L, Rees RC, McArdle SEB. HAGE, a cancer/testis antigen with potential for melanoma immunotherapy: identification of several MHC class I/II HAGE-derived immunogenic peptides. *Cancer Immunol Immunother.* **2007**;56(12):1885–1895. doi: [10.1007/s00262-007-0331-2](https://doi.org/10.1007/s00262-007-0331-2).
45. Autenrieth SE, Warnke P, Wabnitz GH, Lucero Estrada C, Pasquevich KA, Drechsler D, Günter M, Hochweller K, Novakovic A, Beer-Hammer S, et al. Depletion of dendritic cells enhances innate anti-bacterial host defense through modulation of phagocyte homeostasis. *PLOS Pathog.* **2012**;8(2):e1002552. doi: [10.1371/journal.ppat.1002552](https://doi.org/10.1371/journal.ppat.1002552).
46. Uhl P, Helm F, Hofhaus G, Brings S, Kaufman C, Leotta K, Urban S, Haberkorn U, Mier W, Fricker G. A liposomal formulation for the oral application of the investigational hepatitis B drug Myrcludex B. *Eur J Pharm Biopharm.* **2016**;103:159–166. doi: [10.1016/j.ejpb.2016.03.031](https://doi.org/10.1016/j.ejpb.2016.03.031).
47. Lee J, Kang S, Park H, Sun JG, Kim EC, Shim G. Nanoparticles for lymph node-directed delivery. *Pharmaceutics.* **2023**;15(2):565. doi: [10.3390/pharmaceutics15020565](https://doi.org/10.3390/pharmaceutics15020565).
48. He P, Tang H, Zheng Y, Xiong Y, Cheng H, Li J, Zhang Y, Liu G. Advances in nanomedicines for lymphatic imaging and therapy. *J Nanobiotechnol.* **2023**;21(1):292. doi: [10.1186/s12951-023-02022-x](https://doi.org/10.1186/s12951-023-02022-x).
49. Sánchez Jiménez A, Puelles R, Perez-Fernandez M, Barrueta Peña L, Jacobsen NR, Suarez-Merino B, Micheletti C, Manier N, Salieri B, Hischier R, et al. Safe(r) by design guidelines for the nanotechnology industry. *NanoImpact.* **2022**;25:100385. doi: [10.1016/j.impact.2022.100385](https://doi.org/10.1016/j.impact.2022.100385).
50. Blatnik R, Mohan N, Bonsack M, Falkenby LG, Hoppe S, Josef K, Steinbach A, Becker S, Nadler WM, Rucevic M, et al. A targeted LC-MS strategy for low-abundant HLA class-I-presented peptide detection identifies novel human papillomavirus T-cell epitopes. *Proteomics.* **2018**;18(11):e1700390. doi: [10.1002/pmic.201700390](https://doi.org/10.1002/pmic.201700390).
51. Nagarsheth NB, Norberg SM, Sinkoe AL, Adhikary S, Meyer TJ, Lack JB, Warner AC, Schweitzer C, Doran SL, Korrapati S, et al. TCR-engineered T cells targeting E7 for patients with metastatic HPV-associated epithelial cancers. *Nat Med.* **2021**;27(3):419–425. doi: [10.1038/s41591-020-01225-1](https://doi.org/10.1038/s41591-020-01225-1).
52. Allan RS, Waithman J, Bedoui S, Jones CM, Villadangos JA, Zhan Y, Lew AM, Shortman K, Heath WR, Carbone FR. Migratory dendritic cells transfer antigen to a lymph node-resident dendritic cell population for efficient CTL priming. *Immunity.* **2006**;25(1):153–162. doi: [10.1016/j.immuni.2006.04.017](https://doi.org/10.1016/j.immuni.2006.04.017).

53. Nayl AA, Abd-Elhamid AI, Aly AA, Bräse S. Recent progress in the applications of silica-based nanoparticles. *RSC Adv.* **2022**;12(22):13706–13726. doi: [10.1039/D2RA01587K](https://doi.org/10.1039/D2RA01587K).
54. Janjua TI, Cao Y, Kleitz F, Linden M, Yu C, Popat A. Silica nanoparticles: a review of their safety and current strategies to overcome biological barriers. *Adv Drug Delivery Rev.* **2023**;203:115115. doi: [10.1016/j.addr.2023.115115](https://doi.org/10.1016/j.addr.2023.115115).
55. Spitzmüller L, Nitschke F, Rudolph B, Berson J, Schimmel T, Kohl T. Dissolution control and stability improvement of silica nanoparticles in aqueous media. *J Nanopart Res.* **2023**;25(3):40. doi: [10.1007/s11051-023-05688-4](https://doi.org/10.1007/s11051-023-05688-4).
56. Antoniou EE, Nolde J, Torensma B, Dekant W, Zeegers MP. Nine human epidemiological studies on synthetic amorphous silica and respiratory health. *Toxicol Lett.* **2024**;399:12–17. doi: [10.1016/j.toxlet.2023.08.005](https://doi.org/10.1016/j.toxlet.2023.08.005).
57. Geszke-Moritz M, Moritz M. Biodegradable polymeric nanoparticle-based drug delivery systems: comprehensive overview, perspectives and challenges. *Polymers (Basel).* **2024**;16(17):2536. doi: [10.3390/polym16172536](https://doi.org/10.3390/polym16172536).
58. Thi TTH, Suys EJA, Lee JS, Nguyen DH, Park KD, Truong NP. Lipid-based nanoparticles in the clinic and clinical trials: from cancer nanomedicine to COVID-19 vaccines. *Vaccines (Basel).* **2021**;9(4):359. doi: [10.3390/vaccines9040359](https://doi.org/10.3390/vaccines9040359).
59. Wang J, Ding Y, Chong K, Cui M, Cao Z, Tang C, Tian Z, Hu Y, Zhao Y, Jiang S. Recent advances in lipid nanoparticles and their safety concerns for mRNA delivery. *Vaccines (Basel).* **2024**;12(10):1148. doi: [10.3390/vaccines12101148](https://doi.org/10.3390/vaccines12101148).
60. Nakamura T, Kawai M, Sato Y, Maeki M, Tokeshi M, Harashima H. The effect of size and charge of lipid nanoparticles prepared by microfluidic mixing on their lymph node transitivity and distribution. *Mol Pharm.* **2020**;17(3):944–953. doi: [10.1021/acs.molpharmaceut.9b01182](https://doi.org/10.1021/acs.molpharmaceut.9b01182).
61. He R, Zang J, Zhao Y, Dong H, Li Y. Nanotechnology-based approaches to promote lymph node targeted delivery of cancer vaccines. *ACS Biomater Sci Eng.* **2022**;8(2):406–423. doi: [10.1021/acsbiomaterials.1c01274](https://doi.org/10.1021/acsbiomaterials.1c01274).
62. Dubowchik GM, Firestone RA, Padilla L, Willner D, Hofstead SJ, Mosure K, Knipe JO, Lasch SJ, Trail PA. Cathepsin B-labile dipeptide linkers for lysosomal release of doxorubicin from internalizing immunoconjugates: model studies of enzymatic drug release and antigen-specific in vitro anticancer activity. *Bioconjugate Chem.* **2002**;13(4):855–869. doi: [10.1021/bc025536j](https://doi.org/10.1021/bc025536j).
63. Gosalia DN, Salisbury CM, Ellman JA, Diamond SL. High throughput substrate specificity profiling of serine and cysteine proteases using solution-phase fluorogenic peptide microarrays*. *Mol Cell Proteomics.* **2005**;4(5):626–636. doi: [10.1074/mcp.M500004-MCP200](https://doi.org/10.1074/mcp.M500004-MCP200).
64. Choe Y, Leonetti F, Greenbaum DC, Lecaille F, Bogoy M, Brömme D, Ellman JA, Craik CS. Substrate profiling of cysteine proteases using a combinatorial peptide library identifies functionally unique specificities*. *J Biol Chem.* **2006**;281(18):12824–12832. doi: [10.1074/jbc.M513331200](https://doi.org/10.1074/jbc.M513331200).
65. Zhang C, Anderson A, DeLisi C. Structural principles that govern the peptide-binding motifs of class I MHC molecules. *J Mol Biol.* **1998**;281(5):929–947. doi: [10.1006/jmbi.1998.1982](https://doi.org/10.1006/jmbi.1998.1982).
66. Abualrous ET, Saini SK, Ramnarayan VR, Ilca FT, Zacharias M, Springer S. The carboxy terminus of the ligand peptide determines the stability of the MHC class I molecule H-2Kb: a combined molecular dynamics and experimental study. *PLOS ONE.* **2015**;10(8):e0135421. doi: [10.1371/journal.pone.0135421](https://doi.org/10.1371/journal.pone.0135421).
67. Saveanu L, Carroll O, Hassainya Y, Van Endert P. Complexity, contradictions, and conundrums: studying post-proteasomal proteolysis in HLA class I antigen presentation. *Immunol Rev.* **2005**;207(1):42–59. doi: [10.1111/j.0105-2896.2005.00313.x](https://doi.org/10.1111/j.0105-2896.2005.00313.x).
68. Dekhtiarenko I, Ratts RB, Blatnik R, Lee LN, Fischer S, Borkner L, Oduro JD, Marandu TF, Hoppe S, Ruzsics Z, et al. Peptide processing is critical for T-cell memory inflation and may be optimized to improve immune protection by CMV-based vaccine vectors. *PLOS Pathog.* **2016**;12(12):e1006072. doi: [10.1371/journal.ppat.1006072](https://doi.org/10.1371/journal.ppat.1006072).
69. Mempel TR, Henrickson SE, von Andrian UH. T-cell priming by dendritic cells in lymph nodes occurs in three distinct phases. *Nature.* **2004**;427(6970):154–159. doi: [10.1038/nature02238](https://doi.org/10.1038/nature02238).
70. Fu C, Jiang A. Dendritic cells and CD8 T cell immunity in tumor microenvironment. *Front Immunol.* **2018**;9. doi: [10.3389/fimmu.2018.03059](https://doi.org/10.3389/fimmu.2018.03059).
71. Zottnick S, Voß AL, Riemer AB. Inducing immunity where it matters: orthotopic HPV tumor models and therapeutic vaccinations. *Front Immunol.* **2020**;11:1750. doi: [10.3389/fimmu.2020.01750](https://doi.org/10.3389/fimmu.2020.01750).
72. Liu H, Moynihan KD, Zheng Y, Szeto GL, Li AV, Huang B, Van Egeren DS, Park C, Irvine DJ. Structure-based programming of lymph-node targeting in molecular vaccines. *Nature.* **2014**;507(7493):519–522. doi: [10.1038/nature12978](https://doi.org/10.1038/nature12978).
73. Bevan MJ. Helping the CD8+ T-cell response. *Nat Rev Immunol.* **2004**;4(8):595–602. doi: [10.1038/nri1413](https://doi.org/10.1038/nri1413).
74. Kawase K, Taguchi A, Ishizaka A, Lin J, Ueno T, Yoshimoto D, Eguchi S, Mori S, Sone K, Mori M, et al. Allelic loss of HLA class I facilitates evasion from immune surveillance in cervical intraepithelial neoplasia. *HLA.* **2024**;103(6):e15509. doi: [10.1111/tan.15509](https://doi.org/10.1111/tan.15509).
75. Graham SV. The human papillomavirus replication cycle, and its links to cancer progression: a comprehensive review. *Clin Sci.* **2017**;131(17):2201–2221. doi: [10.1042/CS20160786](https://doi.org/10.1042/CS20160786).
76. Ibrahim Khalil A, Zhang L, Muwonge R, Sauvaget C, Basu P. Efficacy and safety of therapeutic HPV vaccines to treat CIN 2/CIN 3 lesions: a systematic review and meta-analysis of phase II/III clinical trials. *BMJ Open.* **2023**;13(10):e069616. doi: [10.1136/bmjopen-2022-069616](https://doi.org/10.1136/bmjopen-2022-069616).

77. Wang R, Huang H, Yu C, Li X, Wang Y, Xie L. Current status and future directions for the development of human papillomavirus vaccines. *Front Immunol.* 2024;15. doi: [10.3389/fimmu.2024.1362770](https://doi.org/10.3389/fimmu.2024.1362770).
78. Campbell JS, Pai SI. Human papillomavirus-directed therapeutics for human papillomavirus-associated oropharyngeal cancer. *Cancer J.* 2022;28(5):407–415. doi: [10.1097/PPO.0000000000000621](https://doi.org/10.1097/PPO.0000000000000621).
79. World Health Organization. WHO preferred product characteristics for therapeutic HPV vaccines <https://www.who.int/publications/i/item/9789240092174>. 2024.